IOP Publishing | London Mathematical Society Nonlinearity

Nonlinearity **33** (2020) 2106–2142 https://doi.org/10.1088/1361-6544/ab6f4f

Slow travelling wave solutions of the nonlocal Fisher-KPP equation

John Billingham

School of Mathematical Sciences, The University of Nottingham, University Park, Nottingham NG7 2RD, United Kingdom

E-mail: John.Billingham@Nottingham.ac.uk

Received 5 July 2019, revised 10 January 2020
Accepted for publication 23 January 2020
Published 16 March 2020

Recommended by Professor Guido Schneider

Abstract

We study travelling wave solutions, $u \equiv U(x-ct)$, of the nonlocal Fisher-KPP equation in one spatial dimension,

$$u_t = Du_{xx} + u\left(1 - \phi * u\right),$$

with $D \ll 1$ and $c \ll 1$, where $\phi * u$ is the spatial convolution of the population density, $u(x,t)$, with a continuous, symmetric, strictly positive kernel, $\phi(x)$, which is decreasing for $x > 0$ and has a finite derivative as $x \to 0^+$, normalized so that $\int_{-\infty}^{\infty} \phi(x)\mathrm{d}x = 1$. In addition, we restrict our attention to kernels for which the spatially-uniform steady state $u = 1$ is stable, so that travelling wave solutions have $U \to 1$ as $x - ct \to -\infty$ and $U \to 0$ as $x - ct \to \infty$ for $c > 0$.

We use the formal method of matched asymptotic expansions and numerical methods to solve the travelling wave equation for various kernels, $\phi(x)$, when $c \ll 1$. The most interesting feature of the leading order solution behind the wavefront is a sequence of tall, narrow spikes with $O(1)$ weight, separated by regions where U is exponentially small. The regularity of $\phi(x)$ at $x = 0$ is a key factor in determining the number and spacing of the spikes, and the spatial extent of the region where spikes exist.

Keywords: nonlocal differential equation, travelling wave solution, matched asymptotic expansions
Mathematics Subject Classification numbers: 34B10, 35K57, 41A60

1. Introduction

In this paper we study travelling wave solutions of the nonlocal Fisher-KPP equation in one spatial dimension,

$$\frac{\partial u}{\partial t} = D\frac{\partial^2 u}{\partial x^2} + u\left(1 - \int_{-\infty}^{\infty} \phi(x-y)u(y,t)\mathrm{d}y\right), \tag{1}$$

where D is a positive constant and the kernel, $\phi(x)$, is continuous, symmetric, strictly positive and decreasing for $x > 0$, with finite derivative as $x \to 0^+$, normalized so that

$$\int_{-\infty}^{\infty} \phi(x)\mathrm{d}x = 1. \tag{2}$$

We are interested in permanent form travelling wave (TW) solutions of (1). Numerical simulations suggest that minimum speed travelling waves are formed in the solution of initial value problems with sufficiently localized initial conditions. We focus on the case $D \ll 1$, which we will see is the limit in which interesting, highly nonlinear behaviour can be found.

TW solutions with speed c are of the form, $u(x,t) \equiv U(z)$, where $z = x - ct$, and satisfy the nonlocal ordinary differential equation

$$-cU_z = DU_{zz} + U\left(1 - \int_{-\infty}^{\infty} \phi(z-y)U(y)\mathrm{d}y\right). \tag{3}$$

We will confine our attention to TW solutions that satisfy

$$U \to 1 \text{ as } z \to -\infty,\ U \to 0 \text{ as } z \to \infty \tag{4}$$

with $c > 0$ by studying kernels for which it is straightforward to show that the uniform solutions $u = 0$ and $u = 1$ of (1) are respectively unstable and stable. TW solutions with these boundary conditions are right-propagating and connect the uniform steady states, $U = 1$ and $U = 0$. Note that discontinuous kernels, [1], and kernels that become negative, [2], can lead to instability of the steady state $u = 1$, as can some smooth positive kernels such as $\phi \propto \mathrm{e}^{-x^4}$ and $\phi \propto (1 + x^4)^{-1}$. Instability of $u = 1$ leads to the existence of periodic travelling wave solutions, which are not the subject of the present work (see, for example, [3]).

The nonlocal Fisher-KPP equation, (1), is relevant to many different scientific areas, [3–5], and has been studied extensively, but mainly through proofs of the existence of travelling wave solutions, [6–8], and in the limit of fast travelling waves ($D \gg 1$). Fast travelling wave solutions are a small perturbation of the travelling wave solution of the local Fisher-KPP equation, which is equivalent to (1) with $\phi(x) = \delta(x)$, [9]. When $D \ll 1$, (1) can be characterised as an equation with short range activation and long range inhibition, which is known to lead to the generation of localized spikes in other reaction-diffusion systems, [10].

It is helpful to work in terms of the variable $L(z) \equiv \log U(z)$, so that (3) and (4) become

$$-cL_z = D\left(L_{zz} + L_z^2\right) + 1 - \int_{-\infty}^{\infty} \phi(z-y)\mathrm{e}^{L(y)}\mathrm{d}y, \tag{5}$$

subject to

$$L \to 0 \text{ as } z \to -\infty,\ L \sim k_+ z \text{ as } z \to \infty, \tag{6}$$

with

$$k_+ \equiv \frac{-c + \sqrt{c^2 - 4D}}{2D}, \tag{7}$$

since the TW solution must connect with the stable manifold of the steady state $U = 0$ as $z \to \infty$. This transformation was also used in [11], which considered the formation of spikes, represented by delta functions, in steady and unsteady solutions of (1) on a finite domain using a kernel with compact support. Equation (7) suggests, as was proved rigorously in [6], that a TW solution with $U > 0$ only exists for $c \geqslant 2\sqrt{D}$. It is therefore convenient to write $D = D_0 c^2$ with $D_0 \leqslant \frac{1}{4}$ and consider the solutions of (5) when $c \ll 1$. We will find below that the diffusive terms in (5) are only significant ahead of the wavefront when $c \ll 1$, and we will later assume that $D_0 = 0$ in order to simplify parts of the asymptotic analysis of the solution behind the wavefront.

We begin in section 2 with a preliminary numerical investigation of the solution of (5) for the two most obvious choices of kernel,

$$\Phi_1(x) \equiv \frac{1}{2}\mathrm{e}^{-|x|}, \ \Phi_\infty(x) \equiv \frac{1}{2\sqrt{\pi}}\mathrm{e}^{-\frac{1}{4}x^2}. \tag{8}$$

This motivates a discussion of how to investigate the very different forms of TW solution in these two cases through choices of kernel that are intermediate between the two, which is presented in section 3. In section 4 we construct the asymptotic solution when $\phi(x)$ has a discontinuous derivative at $x = 0$. We study the kernel $\phi = \Phi_1$ in detail, since it allows (5) to be written as a single ordinary differential equation. We then show how to generalize this analysis to other kernels with discontinuous derivative at $x = 0$ by writing down an ansatz for the behaviour of U for all z, which includes a delta function spike behind the wavefront. We then discuss the asymptotic solution of (5) for other kernels, in particular a family of kernels (discussed in section 3) that allows us to unfold the bifurcation from a single spike solution when $\phi = \Phi_1$ to a solution with infinitely-many spikes that exist in a finite region $z_\infty < z < 0$ when $\phi = \Psi_2 \equiv \frac{1}{4}(1 + |x|)\,\mathrm{e}^{-|x|}$, a kernel that is three-, but not four-, times differentiable at $x = 0$. In section 5 we show that kernels that are twice-, but not infinitely-, differentiable have a similar asymptotic structure to the solution with $\phi = \Psi_2$, and discuss how the region $z_\infty < z < 0$, where the spikes exist, grows as n increases for a family of kernels $\phi = \Phi_n$. We conclude in section 6 that infinitely-many spikes exist in any semi-infinite region $z < z_1$ for all $z_1 < 0$ when $\phi = \Phi_\infty$ and for other infinitely-differentiable kernels.

2. Numerical solutions of the Fisher-KPP travelling wave equation for two typical kernels

Natural choices of kernel, $\phi(x)$, are either the exponential kernel, $\phi = \Phi_1$, or the Gaussian kernel, $\phi = \Phi_\infty$, (8). Although these kernels are most obviously distinguished by the more rapid rate of decay of the latter as $x \to \pm\infty$, we find that it is only their behaviour as $x \to 0$, where the former has a discontinuous derivative and the latter is infinitely-differentiable, that has a significant effect on the qualitative nature of TW solutions of (5) as $c \to 0$. In order to gain some insight into TW solutions of (5), we begin by examining numerical solutions for these two kernels. After truncating to a finite domain, we use central-differences to evaluate the spatial derivatives in (5) and two-point Gaussian quadrature to compute the integral, taking a linear variation in $L(z)$ across each element, collocating at the midpoint. We took the translational invariance of (5) into account by fixing the area under the solution in the truncated domain of solution. We solved the resulting system of nonlinear algebraic equations using *fsolve* in MATLAB, which uses the trust region dogleg method, providing the analytical Jacobian to this routine to increase its execution speed. We proceeded by continuation from

$c = 0.1$ down to a small value of c, using adaptive regridding to resolve the steep gradients of the solution, with the length scale estimated from $\sqrt{U/|U_{zz}|}$ at each local maximum.

The TW solution with kernel $\Phi_1(x)$, wavespeed $c = 10^{-12}$ and diffusion coefficient $D_0 = \frac{1}{4}$ is shown in figure 1. The top panel shows the form of the TW solution on an $O(1)$ lengthscale. There appears to be a single, large, narrow spike at the wavefront. Note that the U-axis has been restricted; the actual maximum value of the spike is close to 3×10^5 as can be seen in the bottom right hand panel, where the z-axis has been restricted so that the full structure of the spike can be seen. Note the asymmetry of the spike, with U decaying more rapidly as z increases than it does as z decreases. The spike contains an approximately unit area, which leads us to believe (correctly, as we shall see) that the leading order solution can be written as $U(z) \sim H(-z) + \delta(z)$ as $c \to 0$, up to a translation in z, with H the Heaviside step function. There is, however, some small scale structure to the solution, as can be seen in the bottom left hand panel of figure 1. There is an additional, smaller asymmetric spike to the left of the large spike, along with some further oscillations as z decreases. Figure 2 shows that the heights of the spikes scale with $c^{-\frac{1}{2}}$ and $c^{-\frac{1}{8}}$, whilst their separation scales with $c^{\frac{1}{4}}$. We will analyse this structure in detail in section 4.1.

We now turn our attention to TW solutions with the kernel Φ_∞. The solution for $c = 10^{-10}$ (note that the existence of so many large spikes means that we are unable to resolve the solution adequately with a reasonable number of grid points for smaller values of c) and $D_0 = \frac{1}{4}$ is shown in figure 3, where it is immediately clear that the structure of the solution is very different to that shown in figure 1. There is a sequence of spikes behind the wavefront with $O(1)$ spacings. The bottom panels of figure 3 suggest that each is locally Gaussian, in contrast to the asymmetric spikes shown in figure 1 when $\phi = \Phi_1$. Figure 4 indicates that the height of each spike scales with $c^{-1/2}$ as $c \to 0$, but decreases with each successive spike (numbered starting from the largest spike, which lies at the wavefront, and proceeding in the direction of decreasing z). The final panels of figure 4 show how the weight, w_m, (computed as the integral of $U(z)$ between successive minima) and spacing, Δz_m, between the spikes behaves with spike number, m. It appears that $w_m \sim \Delta z_m$ as $m \to \infty$, but it is not clear whether Δz_m approaches a finite value or tends to zero very slowly as $m \to \infty$. In either case, this suggests that the spikes fill the region behind the wavefront as $c \to 0$. We will discuss this point further for Φ_∞ and other infinitely-differentiable kernels in section 6.

These numerical solutions of (5) suggest that the structure of the TW solution is very different for these two typical kernels. In the rest of this paper, we will try to understand what controls these differences. We begin by presenting some families of kernels that allow us to unfold the bifurcation structure of the TW solution as the kernel changes from Φ_1 to Φ_∞.

3. Some families of kernels

A fact that we will use extensively in section 4 is that $\Phi_1(x) \equiv \frac{1}{2}\mathrm{e}^{-|x|}$ is a Green's function, since it satisfies

$$\Phi_1 - \frac{\mathrm{d}^2\Phi_1}{\mathrm{d}x^2} = \delta(x). \tag{9}$$

The smooth kernel $\Phi_\infty(x) \equiv \frac{1}{2\sqrt{\pi}}\mathrm{e}^{-\frac{1}{4}x^2}$ is not a Green's function. However, consider the bounded function $\Phi_n(x)$ that satisfies

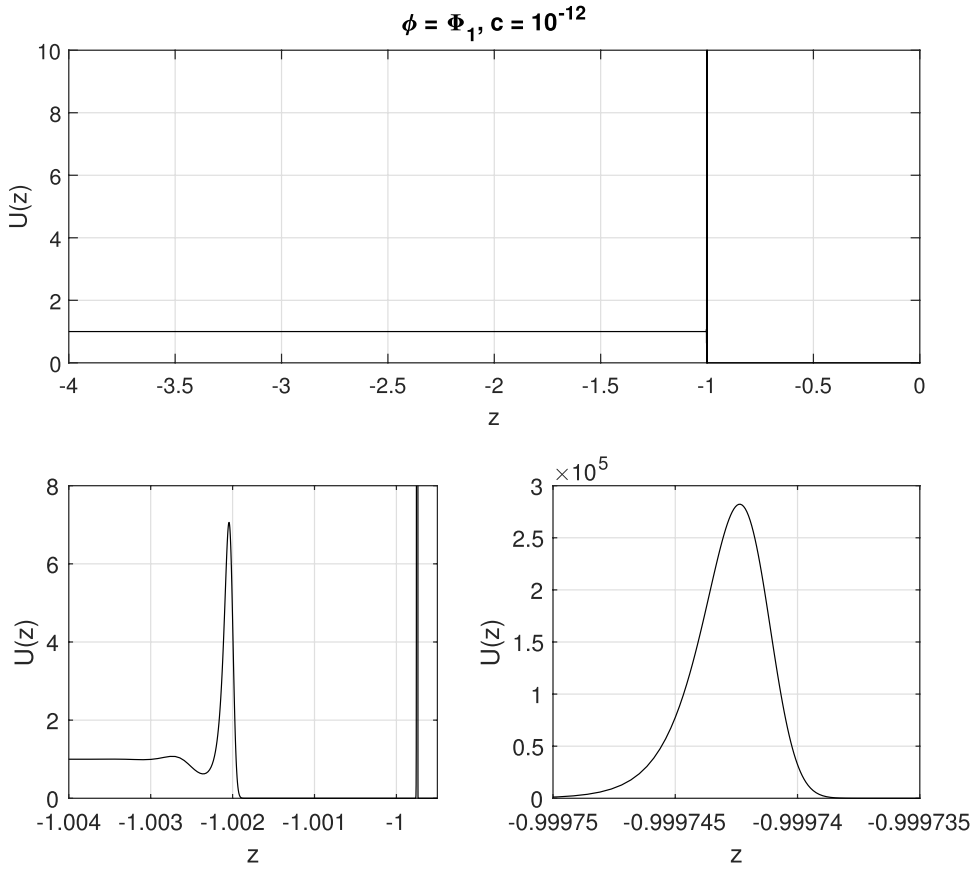

Figure 1. The TW solution with kernel $\Phi_1(x) \equiv \frac{1}{2}\mathrm{e}^{-|x|}$, $c = 10^{-12}$ and $D_0 = \frac{1}{4}$. Note the various restrictions to the axes in the three panels, which highlight different aspects of the structure of the solution.

$$\left(1 - \frac{1}{n}\frac{\mathrm{d}^2}{\mathrm{d}x^2}\right)^n \Phi_n = \delta(x). \tag{10}$$

For positive integer values of n, this is easy to solve analytically, for example,

$$\Phi_2 = \frac{1}{4}\left(\sqrt{2} + 2\,|x|\right)\mathrm{e}^{-\sqrt{2}|x|},\ \Phi_3 = \frac{3\sqrt{3}}{16}\left(1 + \sqrt{3}\,|x| + x^2\right)\mathrm{e}^{-\sqrt{3}|x|}.$$

In general, Φ_n has $2n-2$ continuous derivatives at $x = 0$. The Fourier transform of (10) is

$$\mathcal{F}\left[\Phi_n\right] = \left(1 + \frac{1}{n}k^2\right)^{-n}, \tag{11}$$

and hence

$$\mathcal{F}\left[\Phi_n\right] \sim \mathrm{e}^{-k^2} \text{ as } n \to \infty.$$

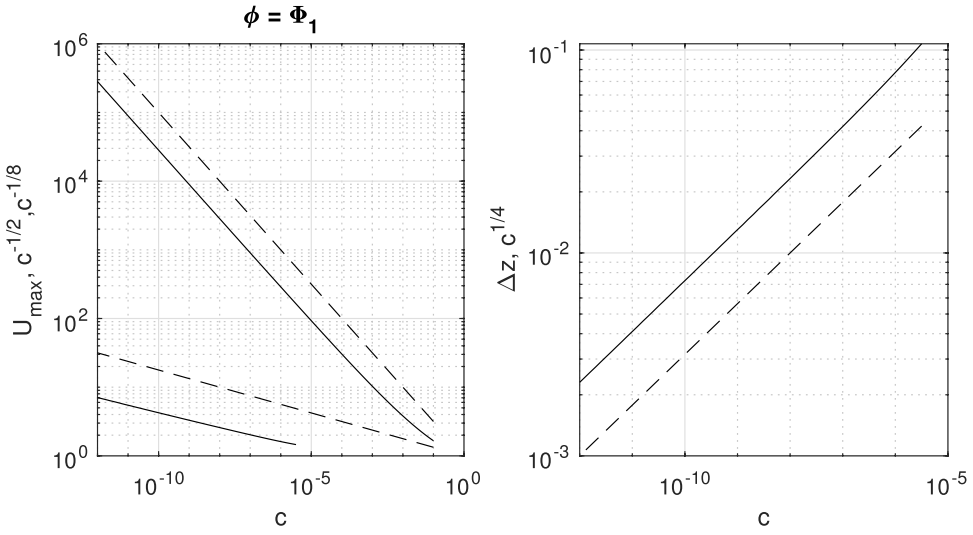

Figure 2. The height (left panel) and separation (right panel) of the two spikes in the TW solution with kernel $\Phi_1(x) \equiv \frac{1}{2}e^{-|x|}$ and $D_0 = \frac{1}{4}$, plotted as functions of c. The solid lines are the heights and separation of the two largest maxima in U, whilst the broken lines are the indicated powers of c.

This shows that it is consistent to define $\Phi_\infty = \frac{1}{2\sqrt{\pi}}e^{-\frac{1}{4}x^2}$, and that the sequence of kernels defined by (10) connects Φ_1 to Φ_∞ as n increases. Moreover, it is also possible to invert (11) for non-integer values of n to obtain the general result,

$$\Phi_n(x) = \frac{n^{\frac{n}{2}+\frac{1}{4}}}{\sqrt{\pi}\Gamma(n)}\left(\frac{1}{2}x\right)^{n-\frac{1}{2}} K_{n-\frac{1}{2}}\left(\sqrt{n}x\right), \tag{12}$$

where $K_{n-\frac{1}{2}}$ is a modified Bessel function of the second kind. This gives us a means of varying a parameter, n, that transforms the kernel Φ_1 to Φ_∞ as $n \to \infty$ whilst smoothly changing the regularity of the function at the origin, since the Taylor series of Φ_n has a non-analytic part of $O(|x|^{2n-1})$ as $|x| \to 0$. The kernel $\Phi_n(x)$ is shown in figure 5 for various values of n.

We will see below that it is also of interest to consider kernels whose slope at the origin varies smoothly without a change of regularity. An obvious candidate is $\phi(x) = (1-k)\,\Phi_1(x) + k\Phi_2(x)$ with $0 \leqslant k \leqslant 1$. However, by defining $\Psi_n(x)$ to be the bounded solution of

$$\left(1 - \frac{\mathrm{d}^2}{\mathrm{d}x^2}\right)^n \Psi_n = \delta(x), \tag{13}$$

and using

$$\tilde{\Phi}_k(x) \equiv (1-k)\,\Phi_1(x) + k\Psi_2(x), \tag{14}$$

a kernel that reduces (5) to a very simple ordinary differential equation, we are able to investigate analytically the effect of changing the slope of $\phi(x)$ at the origin. We will also consider the kernel

$$\bar{\Phi}_k(x) \equiv (1-k)\,\Phi_1(x) + k\Psi_3(x), \tag{15}$$

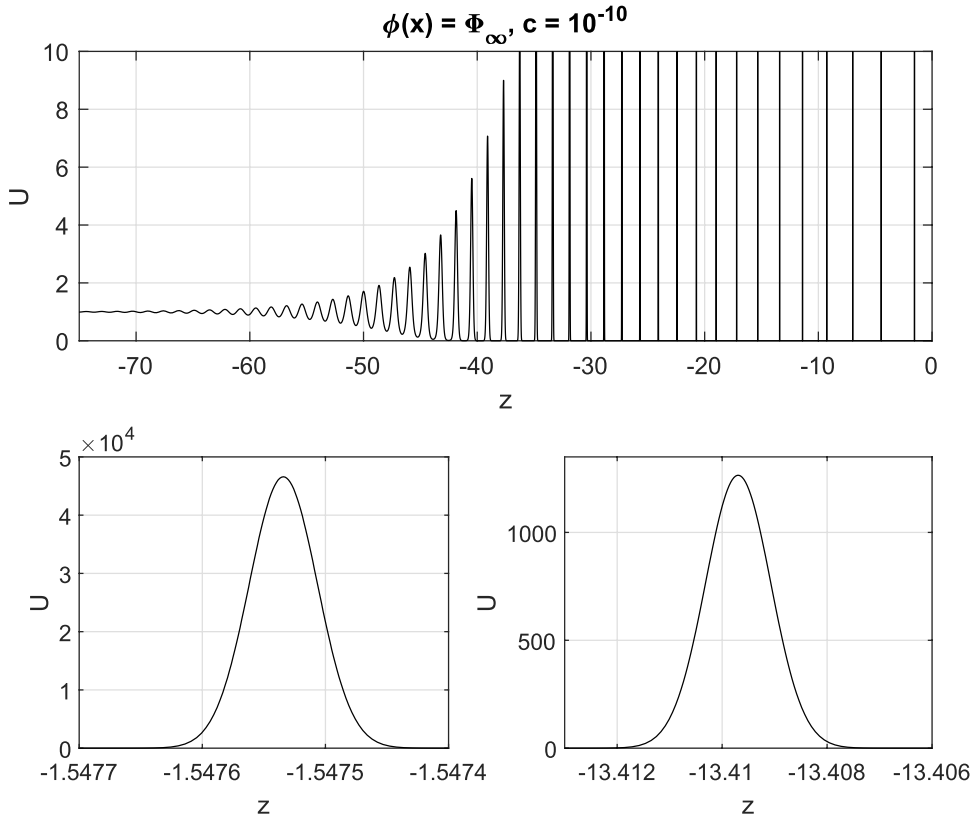

Figure 3. The TW solution for $\phi(x) = \Phi_\infty$, a Gaussian kernel, when $c = 10^{-10}$ and $D_0 = \frac{1}{4}$ (upper panel). The two lower panels show magnified images of the first spike (left panel) and a spike further from the wavefront (right panel). In each case, the profile is locally symmetric and Gaussian. Note the different axes in each panel.

along with a couple of others, to illustrate additional possible features of TW solutions. Note that

$$\Psi_2(x) \equiv \frac{1}{4}\left(1 + |x|\right)\mathrm{e}^{-|x|}, \ \Psi_3(x) \equiv \frac{3}{16}\left(1 + |x| + \frac{1}{3}x^2\right)\mathrm{e}^{-|x|}. \tag{16}$$

The results that we obtain in this paper are summarized in table 1.

4. Kernels that are not twice-differentiable

We begin our investigation of kernels that are not twice-differentiable at the origin by considering $\phi(x) = \Phi_1(x)$ in section 4.1. We then generalize this analysis to similar kernels in section 4.2. In sections 4.3 and 4.4 we study the kernel $\phi(x) = \tilde{\Phi}_k(x)$, and show that, as k increases, a second spike appears when $k = \frac{3}{4}$ and that the number of spikes tends to infinity as $k \to 1$.

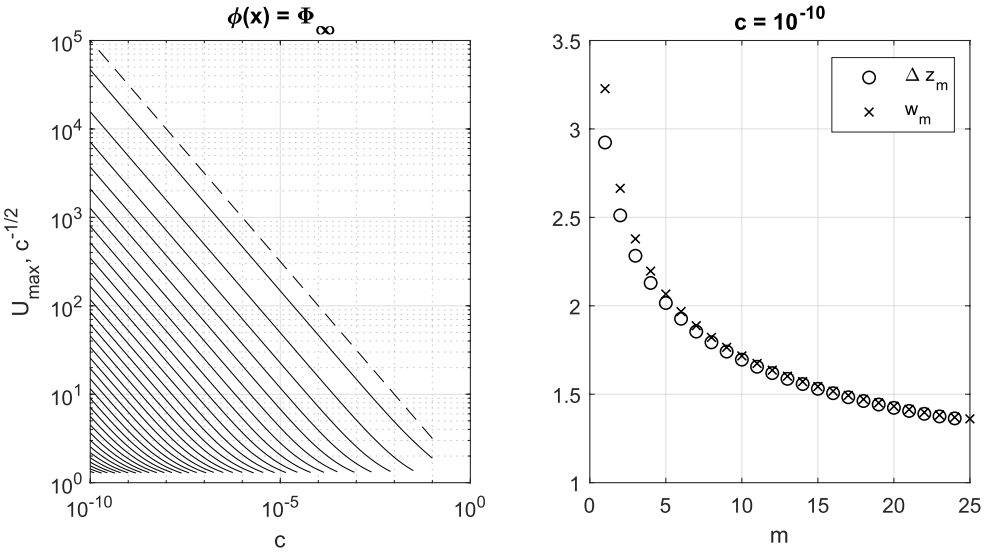

Figure 4. The size of the local maxima of the spikes as a function of c (left panel), and, with $c = 10^{-10}$, separation and weight (right panel) of the spikes as a function of spike number, m, in the TW solution with kernel $\Phi_\infty(x) \equiv \frac{1}{2\sqrt{\pi}} e^{-\frac{1}{4}x^2}$ and $D_0 = \frac{1}{4}$.

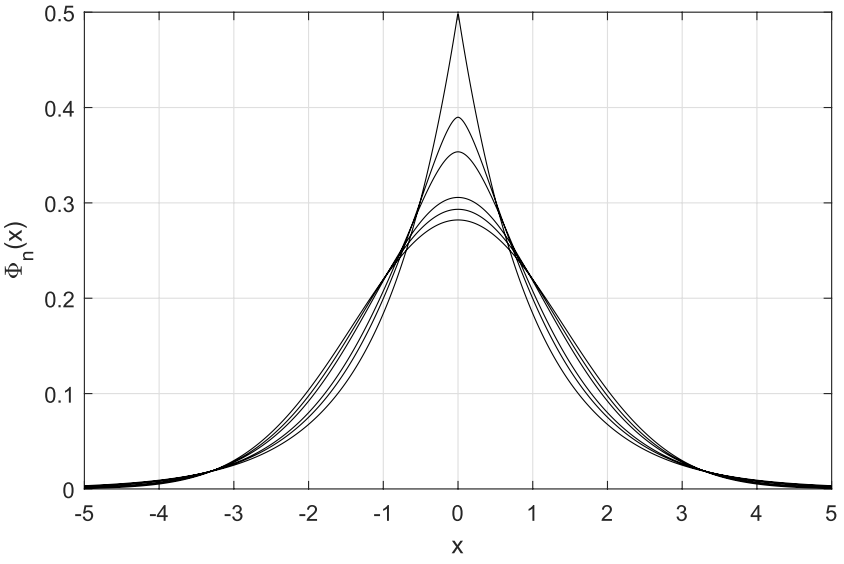

Figure 5. The kernel $\Phi_n(x)$ given by (10) for $n = 1, \frac{3}{2}, 2, 5, 10$ and ∞. Note that $\Phi_n(0)$ is a decreasing function of n.

4.1. Asymptotic solution when $\phi = \Phi_1$ and $c \ll 1$

When $\phi = \Phi_1 \equiv \frac{1}{2}e^{-|x|}$, if we define

$$v \equiv \int_{-\infty}^{\infty} \phi(z - z')e^{L(z')}dz',$$

Table 1. Summary of our main results on TW solutions of (3) as $c \to 0$.

Kernel	Number of spikes with $O(1)$ weight	Extent of region containing spikes
$\Phi_1 \equiv \frac{1}{2}\mathrm{e}^{-\lvert x\rvert}$ Not differentiable	1	$O(c^{1/3})$
e.g. $\tilde{\Phi}_k \equiv \left\{\frac{1}{2}(1-k)+\frac{1}{4}k\,(1+\lvert x\rvert)\right\}\mathrm{e}^{-\lvert x\rvert}$, $\frac{3}{4} < k < 1$	Finite	$O(1)$
Differentiable, but not analytic e.g. Φ_n, Ψ_n, $2 \leqslant n < \infty$	Countably infinite	$O(1)$
Analytic e.g. $\Phi_\infty \equiv \frac{1}{2\sqrt{\pi}}\mathrm{e}^{-\frac{1}{4}x^2}$	Countably infinite	Semi-infinite, $z < 0$

we can use the fact that Φ_1 satisfies (9) to rewrite (5) as

$$-cL_z = D_0c^2\left(L_{zz}+L_z^2\right)+1-v,\ v-v_{zz} = \mathrm{e}^L, \tag{17}$$

and hence, by eliminating v,

$$cL_{zzz}-cL_z = 1-\mathrm{e}^L+D_0c^2\left(L_{zz}+L_z^2-L_{zzzz}-2L_zL_{zzz}-2L_{zz}^2\right), \tag{18}$$

subject to (6). Being able to reformulate (5) as an ordinary differential equation is extremely helpful, as we can use formal asymptotic methods without having to postulate a global form for $U(z) \equiv \mathrm{e}^{L(z)}$ to substitute into the convolution integral.

In its current form, (18) gives $L = 0$ when $c = 0$, which reproduces the boundary condition (6). Two obvious rescalings that bring in more terms at leading order are $L = O(1/c)$, with $L < 0$, $z = O(1)$, which we will find gives the leading order problem ahead of the wavefront, and $L = O(1)$, $z = O(c^{1/3})$, which controls the solution behind the wavefront, and will be the starting point for our analysis. We define

$$L = \tilde{L},\ z = c^{1/3}\tilde{z},$$

with $\tilde{L}$, $\tilde{z} = O(1)$ as $c \to 0$, so that

$$\tilde{L}_{\tilde{z}\tilde{z}\tilde{z}} = 1-\mathrm{e}^{\tilde{L}}+c^{2/3}\tilde{L}_{\tilde{z}}+D_0c^{2/3}\left\{c^{2/3}\left(L_{\tilde{z}\tilde{z}}+L_{\tilde{z}}^2\right)-L_{\tilde{z}\tilde{z}\tilde{z}\tilde{z}}-2L_{\tilde{z}}L_{\tilde{z}\tilde{z}\tilde{z}}-2L_{\tilde{z}\tilde{z}}^2\right\}, \tag{19}$$

subject to

$$\tilde{L} \to 0 \text{ as } \tilde{z} \to -\infty. \tag{20}$$

At leading order,

$$\tilde{L}_{\tilde{z}\tilde{z}\tilde{z}} = 1-\mathrm{e}^{\tilde{L}}. \tag{21}$$

When $\tilde{L} \ll 1$, this gives $\tilde{L}_{\tilde{z}\tilde{z}\tilde{z}} \sim -\tilde{L}$, so that

$$\tilde{L} \sim l_0\mathrm{e}^{\frac{1}{2}\tilde{z}}\cos\left\{\frac{\sqrt{3}}{2}\left(\tilde{z}-\tilde{z}_\infty\right)\right\} \text{ as } \tilde{z} \to -\infty, \tag{22}$$

with l_0 and $\tilde{z}_\infty$ constants. Note that when $\tilde{L}$ is large and negative, $\tilde{L}_{\tilde{z}\tilde{z}\tilde{z}} \sim 1$, so that $\tilde{L}$ increases like $\tilde{z}^3$. When $\tilde{L}$ is large and positive, $\tilde{L}_{\tilde{z}\tilde{z}\tilde{z}}$ is large and negative and $\tilde{L}$ rapidly decreases. These qualitative observations suggest that the oscillations in the solution that are present

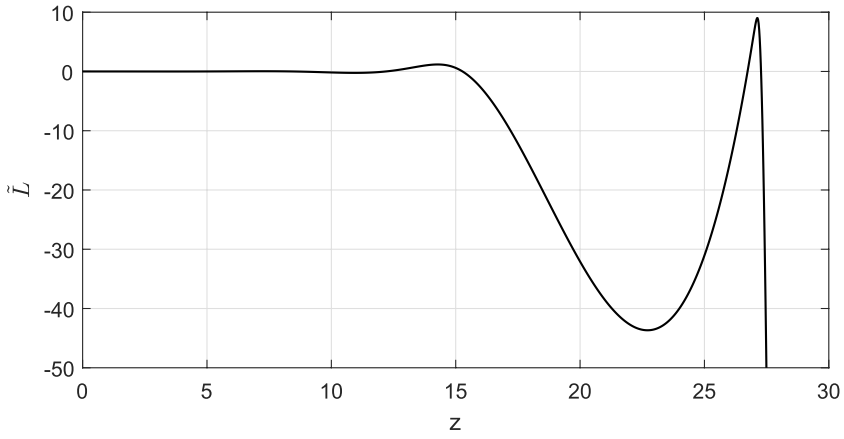

Figure 6. A typical solution of (21). Although we know that the solution cannot have $\tilde{L} \to -\infty$ as $\tilde{z} \to \infty$, it changes so rapidly that the numerical method used, *ode15s* in MATLAB, is unable to compute accurate solutions for $\tilde{L}$ large and negative.

as $\tilde{z} \to -\infty$ persist as $\tilde{L}$ moves away from equilibrium. A typical solution, obtained using *ode15s* in MATLAB, is shown in figure 6 and confirms that the initial oscillations grow as $\tilde{z}$ increases. Although the solution cannot have $\tilde{L} \to -\infty$ as $\tilde{z} \to \infty$, the rapid growth of $-\tilde{L}$ shown in figure 6 means that we are unable to find a numerical solution beyond the value of $\tilde{z}$ shown.

In order to understand how to construct the asymptotic solution of the full problem, we need to understand the structure of solutions such as that shown in figure 6 as $\tilde{L}$ varies between a large negative local minimum, a large positive local maximum and back to a large negative minimum. We can do this by considering the asymptotic solution of (21) subject to the initial conditions

$$\tilde{L} = -\epsilon^{-1},\ \tilde{L}_{\tilde{z}} = 0,\ \tilde{L}_{\tilde{z}\tilde{z}} = \epsilon^{-\frac{1}{3}}\hat{A} > 0 \text{ at } \tilde{z} = 0, \tag{23}$$

with $\hat{A} = O(1)$ as $\epsilon \to 0$, so that we have, without loss of generality, placed a large negative minimum in $\tilde{L}$ with $\tilde{L} = -\epsilon^{-1}$ at $\tilde{z} = 0$. Note that this approach was used in [12, appendix A] to study a similar third order ordinary differential equation. As we shall see, the solution in this case can be constructed as a sequence of asymptotic regions centred on either a local minimum (Region A_m) or a local maximum in $\tilde{L}$ (Region B_m).

4.1.1. Region A_{m+1}. In region A_{m+1}, we rescale using

$$\tilde{L} = \epsilon^{-1}\hat{L},\ \tilde{z} = \epsilon^{-1/3}\hat{z},\ \text{with } \hat{L} < 0,$$

so that

$$\hat{L}_{\hat{z}\hat{z}\hat{z}} = 1 - \mathrm{e}^{\hat{L}/\epsilon}, \tag{24}$$

subject to

$$\hat{L} = -1,\ \hat{L}_{\hat{z}} = 0,\ \hat{L}_{\hat{z}\hat{z}} = \hat{A} \text{ at } \hat{z} = 0. \tag{25}$$

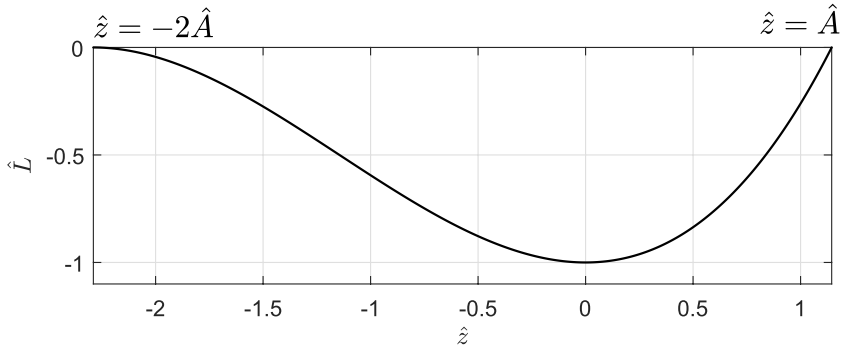

Figure 7. The leading order solution, $\hat{L}(\hat{z})$, in Region A_{m+1}.

To all algebraic orders, this gives

$$\hat{L} = \frac{1}{6}\hat{z}^3 + \frac{1}{2}\hat{A}\hat{z}^2 - 1, \tag{26}$$

which has a local maximum at $\hat{z} = -2\hat{A}$, where $\hat{L} = -1 + \frac{2}{3}\hat{A}^3$. We shall see below that matching to the preceding Region B_{m+1} forces $\hat{L}$ to be zero at this maximum, and hence $\hat{A} \equiv (3/2)^{1/3} \approx 1.145$. This means that the remaining root of (26) is simple, and lies at $\hat{z} = \hat{A}$. The solution is shown in figure 7. As $\hat{z} \to \hat{A}$, $\hat{L} \sim \hat{A}^5(\hat{z} - \hat{A})$, and $\hat{L}$ becomes positive for $\hat{z} > \hat{A}$. We must therefore rescale into a new asymptotic region, which we denote Region B_m.

4.1.2. Region B_m. By matching with Region A_{m+1}, we find that appropriate scalings are

$$\hat{L} = -2\epsilon \log \epsilon + \epsilon \bar{L}, \ \hat{z} = \hat{A} - 2\hat{A}^{-5}\epsilon \log \epsilon + \epsilon \bar{z},$$

with $\bar{L}$, $\bar{z} = O(1)$ as $\epsilon \to 0$. In terms of these scaled variables, (24) becomes

$$\bar{L}_{\bar{z}\bar{z}\bar{z}} = \epsilon^2 - \mathrm{e}^{\bar{L}}. \tag{27}$$

In this region we need to develop a two term asymptotic expansion, so we write

$$\bar{L} = \bar{L}_0 + \epsilon^2 \bar{L}_1 + O(\epsilon^4), \tag{28}$$

with $\bar{L}_0$, $\bar{L}_1 = O(1)$ as $\epsilon \to 0$. At leading order, we have

$$\bar{L}_{0\bar{z}\bar{z}\bar{z}} = -\mathrm{e}^{\bar{L}_0}, \tag{29}$$

subject to the matching condition

$$\bar{L}_0 \sim \hat{A}^5 \bar{z} \ \text{ as } \bar{z} \to -\infty. \tag{30}$$

Note that (29) is invariant under the transformation

$$\bar{z} \to \lambda \bar{z}, \ \bar{L}_0 \to \bar{L}_0 - 3 \log \lambda. \tag{31}$$

Although this does not allow us to solve (29) analytically, we can solve (29) numerically subject to the generic boundary condition

$$\bar{L}_0 \sim \bar{z} \text{ as } \bar{z} \to -\infty, \tag{32}$$

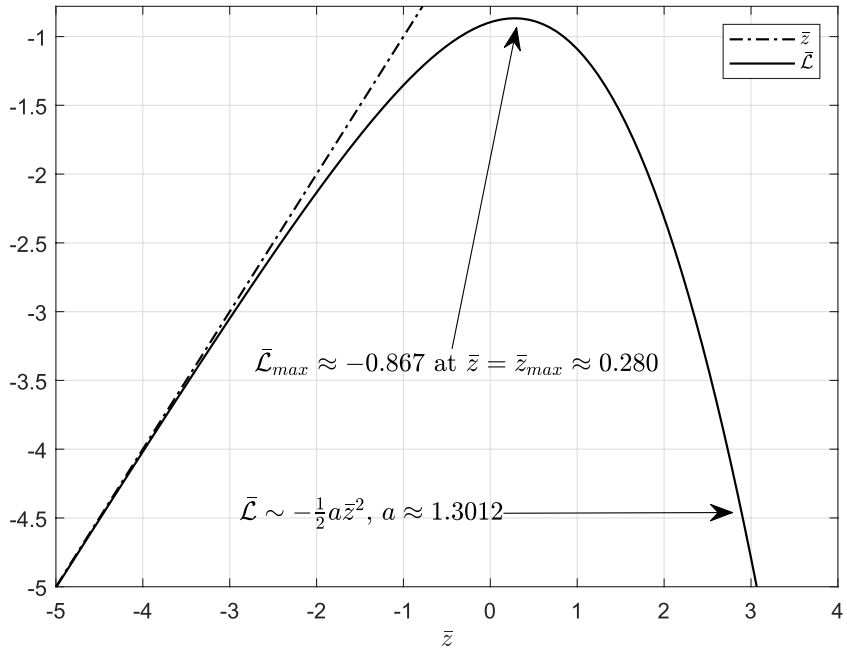

Figure 8. The solution $\bar{\mathcal{L}}(\bar{z})$ that satisfies (29) subject to (32) in Region B_m.

to obtain the solution $\bar{L}_0(\bar{z}) = \bar{\mathcal{L}}(\bar{z})$, which is shown in figure 8. This has maximum value $\bar{\mathcal{L}}_{\max} \approx -0.867$. For $\bar{\mathcal{L}}$ large and negative, $e^{\bar{\mathcal{L}}}$ is exponentially small, so $\bar{\mathcal{L}} \sim -\frac{1}{2}a\bar{z}^2$ as $\bar{z} \to \infty$, and we find that $a \approx 1.302$. It is this asymmetry in the behaviour of $\bar{L}$ in Region B_m that leads to the asymmetry of the spike in the TW solution, shown in figure 1. From the boundary condition (30) and the invariance (31), we can see that

$$\bar{L}_0(\bar{z}) = \bar{\mathcal{L}}(\hat{A}^5\bar{z}) + 15\log\hat{A},$$

which has a maximum value $\bar{L}_{\max} = \bar{\mathcal{L}}_{\max} + 15\log\hat{A} \approx 1.160$. As $\bar{z} \to \infty$, $\bar{L}_0 \sim -\frac{1}{2}\bar{a}\bar{z}^2$, with $\bar{a} \equiv \hat{A}^{10}a \approx 5.030$.

At $O(\epsilon^2)$ we have

$$\bar{L}_{1\bar{z}\bar{z}\bar{z}} = 1 - e^{\bar{L}_0}\bar{L}_1,$$

and hence $\bar{L}_1 \sim \frac{1}{6}\bar{z}^3$ as $\bar{z} \to \infty$. This shows that

$$\bar{L} \sim -\frac{1}{2}\bar{a}\bar{z}^2 + \frac{1}{6}\epsilon^2\bar{z}^3 \text{ as } \bar{z} \to \infty$$

for $\epsilon \ll 1$. This expansion becomes non-uniform when $\bar{z} = O(\epsilon^{-2})$, $\bar{L} = O(\epsilon^{-4})$, and we must rescale into a new asymptotic region, which we label Region A_m.

4.1.3. Region A_m. We define new scaled variables

$$\bar{L} = \epsilon^{-4}\bar{\bar{L}},\ \bar{z} = \epsilon^{-2}\bar{\bar{z}},$$

with $\bar{\bar{L}}$, $\bar{\bar{z}} = O(1)$ as $\epsilon \to 0$, so that (27) becomes

$$\bar{\bar{L}}_{\bar{\bar{z}}\bar{\bar{z}}\bar{\bar{z}}\bar{\bar{z}}} = 1 - \epsilon^{-2}e^{\bar{\bar{L}}/\epsilon^4}. \tag{33}$$

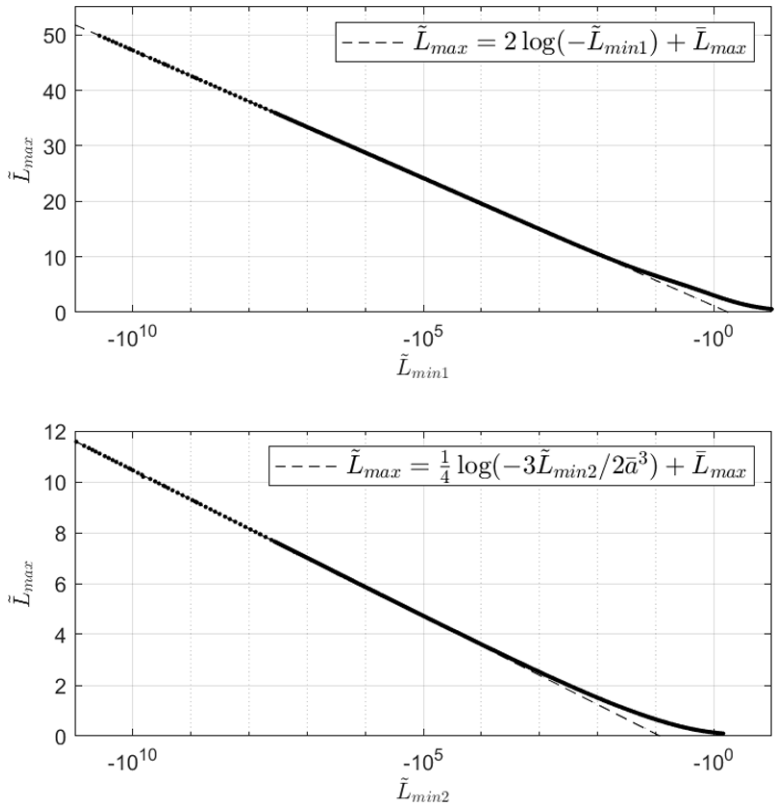

Figure 9. Minima and preceding/following maxima (upper/lower panel). Also shown as broken lines are the leading order asymptotic expressions given by (34) to (36),which are in excellent agreement as $\tilde{L}_{\max} \to \infty$.

At leading order

$$\bar{\bar{L}}_{\bar{\bar{z}}\bar{\bar{z}}\bar{\bar{z}}} = 1,$$

to be solved subject to the matching condition

$$\bar{\bar{L}} \sim -\frac{1}{2}\bar{a}\bar{\bar{z}}^2 \text{ as } \bar{\bar{z}} \to 0.$$

This has solution

$$\bar{\bar{L}} = \frac{1}{6}\bar{\bar{z}}^3 - \frac{1}{2}\bar{a}\bar{\bar{z}}^2,$$

with a minimum of $\bar{\bar{L}}_{\min} = -\frac{2}{3}\bar{a}$ at $\bar{\bar{z}} = 2\bar{a}$.

By matching the solutions in Regions A_m and A_{m+1}, where $\tilde{L}$ is cubic at leading order, through Region B_m, we have been able to obtain the leading order asymptotic values of the maximum and minimum in $\tilde{L}$ that follow a large, negative minimum in $\tilde{L}$. After rewriting the solutions in terms of the original variable, $\tilde{L}$, we find that after the first minimum,

$$\tilde{L} = \tilde{L}_{\min 1} \equiv -\epsilon^{-1}, \tag{34}$$

the following maximum is

$$\tilde{L} = \tilde{L}_{\max} = -2\log\epsilon + \bar{L}_{\max} \approx -2\log\epsilon + 1.160, \tag{35}$$

and the following minimum

$$\tilde{L} = \tilde{L}_{\min 2} \equiv -\frac{2}{3}\bar{a}^3\epsilon^{-4} \approx -84.84\epsilon^{-4}. \tag{36}$$

This shows that a deep minimum is followed by a moderate maximum, and then a much deeper minimum, as can be seen in figure 6. By solving (19) subject to (22) for various values of l_0 and $\tilde{z}_0$, we can plot the values of the maxima and minima of $\tilde{L}$ in figure 9 and find excellent agreement between the numerical solution and the leading order asymptotic solutions, (34) to (36). Note the huge difference in size between the maxima and minima. For example, when $\tilde{L}_{\max} \approx 3$, $U \approx 20$, whilst $\tilde{L}_{\min 2} \approx -3100$ so that $U \approx 5 \times 10^{-1347}$. It is this disparity in scales that leads to the sequence of spikes of rapidly decreasing height that we discuss below.

4.1.4. Region A_1. We have constructed an infinite sequence of asymptotic regions, A_m and B_m, with $m = 1, 2, \ldots$. The final step is to determine how to choose the artificial parameter ϵ so that the terms of $O(c^{2/3})$ in (19), which are neglected in the analysis above, become active in Region A_1. By considering the size of these terms after rescaling, we find that we need $\epsilon = O(c^{1/4})$ as $c \to 0$, so without loss of generality we take $\epsilon = c^{\frac{1}{4}}$. The leading order problem in Region A_1 is then

$$\bar{\bar{L}}_{\bar{\bar{z}}\bar{\bar{z}}\bar{\bar{z}}} - \bar{\bar{L}}_{\bar{\bar{z}}} = 1 + D_0\left(\bar{\bar{L}}_{\bar{\bar{z}}}^2 - 2\bar{\bar{L}}_{\bar{\bar{z}}}\bar{\bar{L}}_{\bar{\bar{z}}\bar{\bar{z}}\bar{\bar{z}}} - 2\bar{\bar{L}}_{\bar{\bar{z}}\bar{\bar{z}}}^2\right),$$

which, using the fact that it comes from (17), can be written as

$$\left(D_0\bar{\bar{L}}_{\bar{\bar{z}}}^2 + \bar{\bar{L}}_{\bar{\bar{z}}} + 1\right)_{\bar{\bar{z}}\bar{\bar{z}}} - \left(D_0\bar{\bar{L}}_{\bar{\bar{z}}}^2 + \bar{\bar{L}}_{\bar{\bar{z}}} + 1\right) = 0,$$

with solution

$$\bar{\bar{L}} = \int_0^{\bar{\bar{z}}} \frac{-1 + \sqrt{1 - 4D_0\left(1 - \mathrm{e}^{-s}\right)}}{2D_0} ds.$$

Note that this has $\bar{\bar{L}} \sim -\frac{1}{2}\bar{\bar{z}}^2$ as $\bar{\bar{z}} \to 0$. The factor of $\bar{a}$ has been scaled back into the solution in the other asymptotic regions, but we omit the details here (see section 4.2 for the general case). In addition, $\bar{\bar{L}} \sim k_+\bar{\bar{z}}$ as $\bar{\bar{z}} \to \infty$, where the solution remains uniform. The constant k_+ is defined in (7), and it is here, ahead of the wavefront, that the minimum wave speed condition, $c \geqslant 2\sqrt{D}$, and hence $D_0 \leqslant \frac{1}{4}$, is determined.

We now know the asymptotic scalings for the successive Regions A_{m+1}, B_m and A_m, along with the fact that $\epsilon = c^{1/4}$ in Region A_1. The scalings of $\tilde{z}$ in the Regions A_m give the distances between the sequence of spikes, whilst the scalings of $\tilde{z}$, L and hence U, in the Regions B_m give the widths and heights of the spikes. By comparing successive Regions A_m, we find that, in terms of $\tilde{z} = c^{-1/3}z$, the (large) width decreases by a fourth root, as does the size of L as m increases to $m + 1$. The width of the spike Region B_m scales with the inverse square root of the width of Region A_m, whilst the size of U in Region B_m scales with the square root of the size of L in Region A_m. When we put all of this together in terms of the original variables, z and $U = \mathrm{e}^L$, we find that the asymptotic scalings are:

$$\text{In Region } A_m: \; z = O\left(c^{\frac{1}{3}\left(1-2^{-2(m-1)}\right)}\right), \; L = O\left(c^{-2^{-2(m-1)}}\right). \tag{37}$$

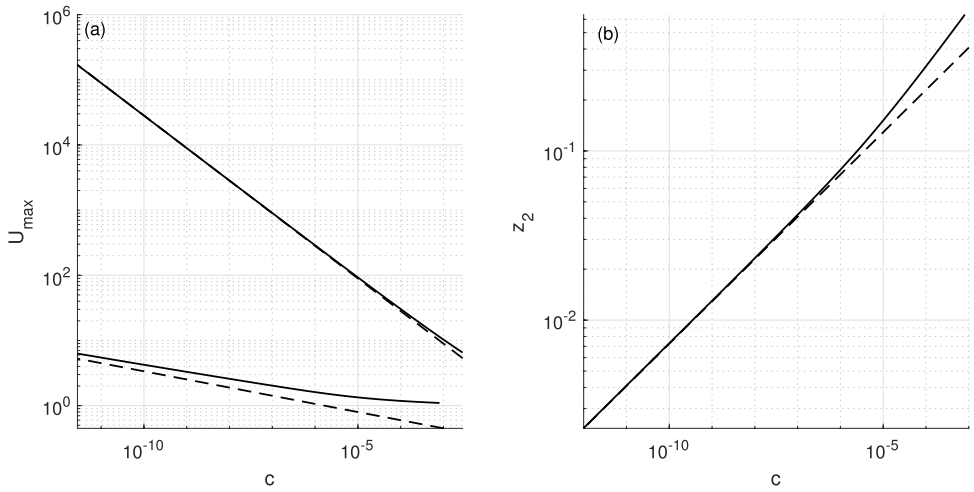

Figure 10. (a) The height of the first two spikes in the solution for $\phi = \Phi_1$. The broken lines show the asymptotic approximations $U_{\max_1} \sim \mathrm{e}^{\bar{L}_{\max}} a^{-3/2} \approx 0.283\, c^{-1/2}$ and $U_{\max_2} \sim \mathrm{e}^{\bar{L}_{\max}} (2/3)^{3/4} a^{-15/8} c^{-1/8} \approx 0.189\, c^{-1/8}$ as $c \to 0$. (b) The distance between the first two spikes. The broken line shows the asymptotic approximation $z_2 \sim 6^{1/2} a^{-1/4}\, c^{1/4} \approx 2.294\, c^{1/4}$ as $c \to 0$.

$$\text{In Region B}_m : \; z = O\left(c^{\frac{1}{3}\left(1+2^{-(2m-1)}\right)}\right), \; U = O\left(c^{-2^{-(2m-1)}}\right). \tag{38}$$

Specifically, in successive Regions A_m, $z = O(1)$, $z = O(c^{1/4})$, $z = O(c^{15/48})$, …, which gives the spacings between the spike Regions B_m. The solution in each Region B_m, viewed in terms of the population density, $U = \mathrm{e}^L$, takes the form of a spike of width and height given by (38), specifically, height $U = O(c^{-1/2})$, $O(c^{-1/8})$, $O(c^{-1/32})$, … and width $z = O(c^{1/2})$, $O(c^{3/8})$, $O(c^{5/16})$, …. The integral of U over each scaled Region B_m, which we refer to as the weight of the spike, is of $O\left(c^{\frac{1}{3}\left(1-2^{-(2m-2)}\right)}\right)$, specifically of $O(1)$, $O(c^{1/4})$, $O(c^{5/16})$, ….

To summarize, the solution consists of a sequence of spikes in the neighbourhood of $z = z_m = O\left(c^{\frac{1}{3}\left(1-2^{-2(m-1)}\right)}\right)$ of decreasing weight and separation as m increases, as $c \to 0$, in apparent contradiction of the form of the solution shown in figure 1. However, the scalings for the mth spike are only asymptotic provided that c is small enough that the height of the spike is large, so that the number of spikes in the solution is

$$m \approx m_0(c) \equiv \frac{\log(-\log c)}{\log 4}. \tag{39}$$

For $c = 10^{-12}$, the value used in figure 1, $m_0(c) \approx 2.4$, so we see just two spikes. For $z < z_{m_0}$, the solution has $L \ll 1$, and hence $U \sim 1$, at leading order. To obtain, for example, $m_0 \approx 3$, we would need $c \approx 10^{-28}$ so, for all practical purposes, there are no more than two clearly defined spikes. Figure 10(a) shows the numerically-calculated heights of the first two spikes in U and their leading order asymptotic approximations. The agreement is very good, noting that the second spike has height of $O(c^{-1/8})$ and is far slower to converge to the leading order approximation than the first spike. Figure 10(b) shows the numerically-calculated spacing between the first two spikes, which is also in excellent agreement with the leading order asymptotic solution.

4.2. Generalization to other non-differentiable kernels

We have been able to construct a complete asymptotic solution when $\phi = \Phi_1 \equiv \frac{1}{2}\mathrm{e}^{-|x|}$ because this is the Green's function for a simple, constant coefficient, ordinary differential equation, so that (5) can be written as a single ordinary differential equation. If ϕ is not twice-differentiable at the origin but not a Green's function, and we can formally write

$$\phi''(x) = -\kappa\delta(x) + \bar{\phi}''(x), \tag{40}$$

where $\bar{\phi}''(x) \equiv \phi''(x)$ for $x \neq 0$, $\bar{\phi}''(0) = \lim_{x\to 0^{\pm}} \phi''(x)$ and

$$\kappa \equiv -2\phi'(0^+) > 0, \tag{41}$$

we can show that the asymptotic structure of the solution is qualitatively the same as for $\phi = \Phi_1$ (note that for $\phi = \Phi_1$, $\kappa = 1$). This means that after differentiating (5) twice we obtain

$$cL_{zzz} = -\kappa\mathrm{e}^L + \int_{-\infty}^{\infty} \bar{\phi}''(z-z')\mathrm{e}^{L(z')}\mathrm{d}z' + D_0c^2\left(L_{zz} + L_z^2\right)_{zz}. \tag{42}$$

We can now proceed by using the ansatz

$$U \equiv \mathrm{e}^L \sim U_\infty(z)H(-z) + w_1\delta(z) \text{ as } c \to 0. \tag{43}$$

In other words, we assume that the leading order structure of the solution is the same as that for $\phi = \Phi_1$. If this gives a consistent asymptotic solution, we have a post hoc justification for using (43). In (43), the function $U_\infty(z)$ is the leading order solution for $-z \gg c^{1/3}$. When $\phi = \Phi_1$, $U_\infty = 1$, but for other kernels, U_∞ need not be constant.

On substituting (43) into (5) and (42), we obtain

$$-cL_z \sim 1 - \int_{-\infty}^{0} U_\infty(z')\phi(z-z')\,\mathrm{d}z' - w_1\phi(z) + D_0c^2\left(L_{zz} + L_z^2\right), \tag{44}$$

and

$$cL_{zzz} + \kappa\mathrm{e}^L \sim \int_{-\infty}^{0} U_\infty(z')\bar{\phi}''(z-z')\,\mathrm{d}z' + w_1\bar{\phi}''(z) + D_0c^2\left(L_{zz} + L_z^2\right)_{zz}. \tag{45}$$

It now becomes clear after using the scalings (37) and (38) that, apart from some differences in constant terms, we recover the same leading order problems and structure that define the solution when $\phi = \Phi_1$. Specifically, in Region A_1, where $L = O(c^{-1})$ and $z = O(1)$, the solution of (44) matches with the solution in Region B_1 provided that $L_z(0) = 0$, so that

$$w_1 = \frac{1}{\phi(0)}\left(1 - \int_{-\infty}^{0} U_\infty(z')\phi(z')\,\mathrm{d}z'\right). \tag{46}$$

In the far field, for $-z \gg c^{1/3}$, where $L \ll 1$, (44) and (46) show that $\bar{U}(z) \equiv U_\infty(z) - 1$ satisfies the integral equation

$$\int_{-\infty}^{0} \bar{U}(z')\phi(z-z')\,\mathrm{d}z' + \left(\frac{1}{2} - \int_{-\infty}^{0} \bar{U}(z')\phi(z')\,\mathrm{d}z'\right)\frac{\phi(z)}{\phi(0)} = \int_{-z}^{\infty} \phi(z')\mathrm{d}z'. \tag{47}$$

Note that when $\phi = \Phi_1$, (47) has solution $U_\infty = 1$, $\bar{U} = 0$. Indeed, (47) shows that the only kernel that leads to the constant solution $U_\infty = 1$ is $\phi = \Phi_1$ and scalings thereof.

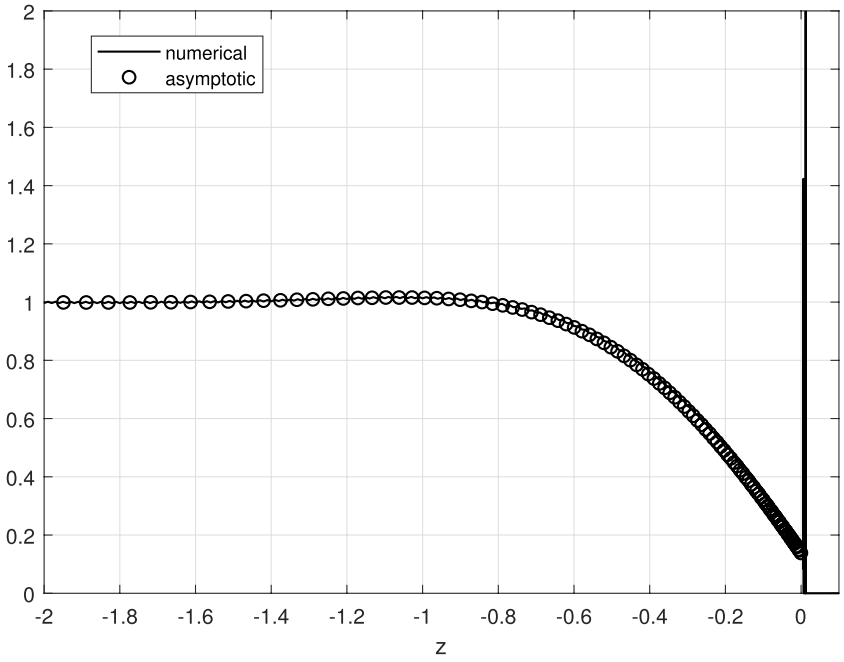

Figure 11. The asymptotic solution as $c \to 0$, $U = U_\infty(z)$ and the numerical solution of the full travelling wave equation, (5) with $c = 10^{-12}$ for the kernel given by (48).

To illustrate how this works, we solved (47) numerically, using the trapezium rule to evaluate the integrals, for the kernel

$$\phi(x) = \frac{1}{\operatorname{erfc}\left(\frac{1}{2}\right)\sqrt{\pi}} \mathrm{e}^{-|x|-x^2-\frac{1}{4}}. \tag{48}$$

The asymptotic solution, along with the numerical solution for $c = 10^{-12}$, is shown in figure 11, and the agreement is excellent. The numerical solution of the full problem also shows the spike at $z = 0$ which appears as a delta function when $z = O(1)$ as $c \to 0$. We use the kernel (48) to illustrate, firstly that this asymptotic solution structure correctly describes the solution for a kernel that does not allow (5) to be reduced to an ordinary differential equation, and secondly that, since this kernel decays like a Gaussian as $|x| \to \infty$, the far field behaviour of the kernel is not its most important feature; the behaviour in the neighbourhood of the origin determines the structure of the solution as $c \to 0$.

In Regions B_m, where the spikes exist, (45) shows that the leading order equation is

$$cL_{zzz} = -\kappa \mathrm{e}^L.$$

After scaling z to remove the factor of κ, this is the leading order equation that we found for $\phi = \Phi_1$. In Regions A_m with $m > 1$, (45) gives

$$cL_{zzz} = A \equiv \int_{-\infty}^{0} U_\infty(z')\bar{\phi}''(z')\,\mathrm{d}z' + w_1\bar{\phi}''(0),$$

at leading order as $c \to 0$. Note that for $\phi = \Phi_1$, $A = 1$ and that for the kernel given by (48), $A \approx 0.255$. The solution is again cubic in z, and the whole asymptotic structure is the same.

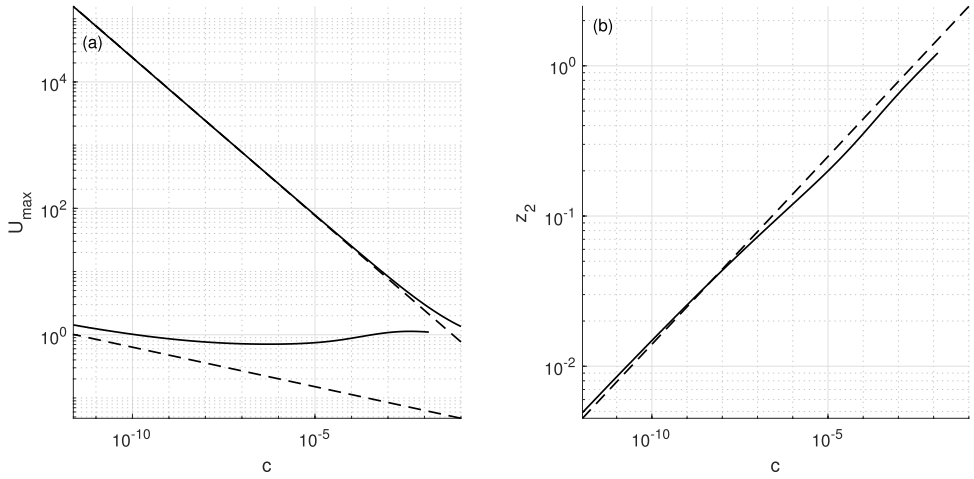

Figure 12. (a) The height of the first two spikes in the solution for the kernel given by (48). The broken lines show the asymptotic approximations $U_{\max_1} \sim 0.243\, c^{-1/2}$ and $U_{\max_2} \sim 0.0357\, c^{-1/8}$ as $c \to 0$. (b) The distance between the first two spikes. The broken line shows the asymptotic approximation $z_2 \sim 4.426 c^{1/4}$ as $c \to 0$.

By matching together these asymptotic regions we are able to obtain the leading order asymptotic solution and in particular show that, if we define

$$\kappa_1 = \int_{-\infty}^{0} U_\infty(z')\phi'(z')\mathrm{d}z' - w_1\phi'(0^+),\ \kappa_m = \left(\frac{2}{3}\right)^{1/2} \frac{A^{1/2}}{a^{1/4}\kappa^{1/6}}\kappa_{m-1}^{1/4} \text{ for } m > 1. \tag{49}$$

Region B_m lies at $z = z_m$, where

$$z_1 \equiv 0,\ z_m \sim -\frac{3\kappa_m}{A} c^{\frac{1}{3}\left(1-2^{-2(m-1)}\right)} \text{ for } m > 1, \tag{50}$$

with local maximum $U = U_{\max_m}$, where

$$U_{\max_m} \sim c^{-2^{-(2m-1)}} \mathrm{e}^{\bar{L}_{\max}} \frac{\kappa_m^{3/2}}{\kappa a^{3/2}} \tag{51}$$

as $c \to 0$. Figure 10 shows the excellent agreement between these leading order asymptotic expressions for $\phi = \Phi_1$. Figures 12 shows the same comparisons for the kernel given by (48) which are also in good agreement, although the rate of convergence is somewhat slower for the second spike.

4.3. Numerical solution for $\phi = \tilde{\Phi}_k$

Although it appears at first sight that we now have a complete asymptotic theory, there are other possibilities, which we can investigate by considering the kernel $\tilde{\Phi}_k(x)$ defined by (14). The slope of this kernel changes by $(1-k)$ at $x = 0$, and $\tilde{\Psi}_k = \Psi_2$ when $k = 1$. Figure 13 shows the travelling wave solution for $c = 10^{-12}$ and various values of k. For $k < k_1$ (we will demonstrate below that $k_1 = \frac{3}{4}$), the structure of the TW solution is of the form (43), with a single spike of $O(1)$ weight separating regions where $U > 0$ and $U = 0$. However, as $k \to k_1$, $U_\infty(0) \to 0$ and as k increases past k_1 a new spike of $O(1)$ weight is formed. The original

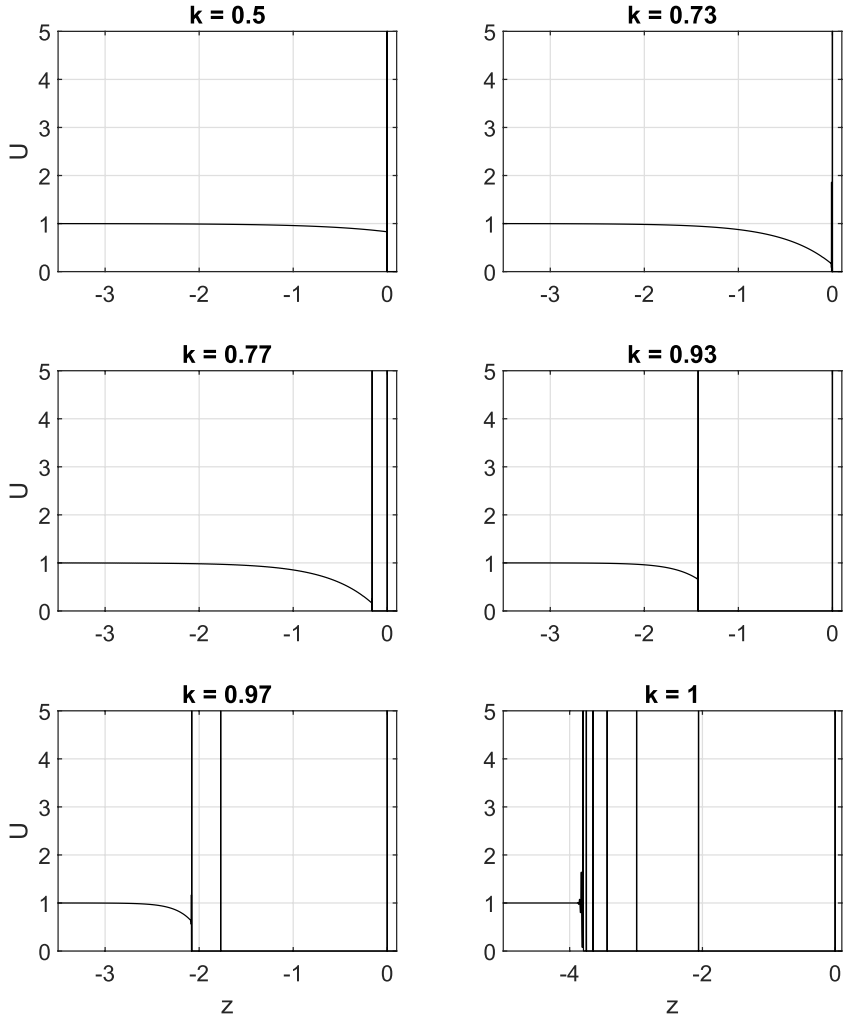

Figure 13. The TW solution for $\phi = \tilde{\Phi}_k$ when $c = 10^{-12}$ and $k = 0.5, 0.73, 0.77, 0.93, 0.97$ and 1.

spike remains, isolated at $z = z_1$, whilst the new spike, at $z = z_2$, has the sequence of small spikes of decreasing height to its left at $z = z_m$ with $m > 2$.

These numerical solutions suggest that there exists a strictly increasing sequence, k_M, with $k_0 = 0$ and $k_M \to 1$ as $M \to \infty$, and, for $k_{M-1} < k < k_M$, a strictly decreasing sequence $z_m(k)$ for $m = 1, 2, \ldots M$, with $z_M \to z_\infty > -\infty$ as $M \to \infty$, such that the leading order asymptotic solution for $c \ll 1$ is

$$U(z;k) = U_\infty(z;k)H(z_M - z) + \sum_{m=1}^{M} w_m \delta(z - z_m) \text{ for } k_{M-1} < k < k_M. \qquad (52)$$

In addition, the sequence of small spikes, with small weight as $c \to 0$, lies at $z = z_m$ with $m > M$, to the left of the final spike of $O(1)$ weight at $z = z_M$. As this notation suggests, it seems natural to think of the solution as consisting of an infinite sequence of spikes at $z = z_m$,

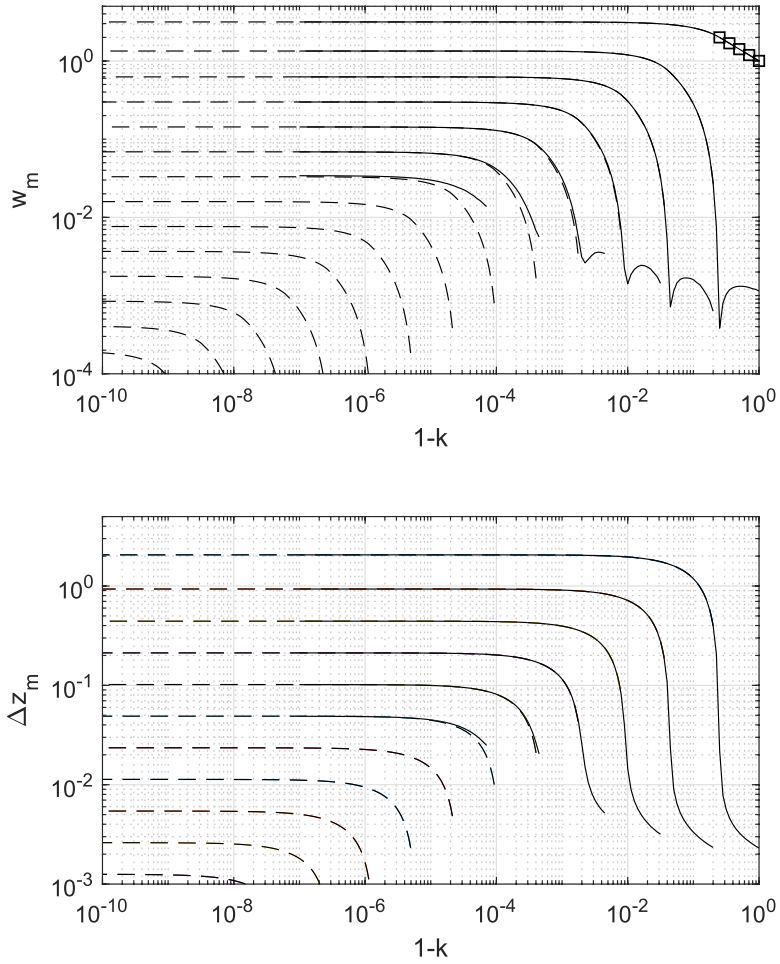

Figure 14. The weight, w_m, and spacing, Δz_m, of the spikes for $\phi = \tilde{\Psi}_k$. The solid lines shows the numerical solution with $c = 10^{-12}$ whilst the broken lines show the asymptotic solution as $c \to 0$. The squares show the analytical expression for the leading order asymptotic weight, w_1, given by (57) for $1 - k > 1 - k_1 = \frac{1}{4}$.

with the functional form of the kernel controlling which of these have weight of $O(1)$ as $c \to 0$.

The solid lines in figure 14 show the weights, $w_m(k)$, and spacings, $\Delta z_m(k) = z_m - z_{m+1}$, for the travelling wave solution with $c = 10^{-12}$ as a function of k, which illustrates the emergence of seven distinct spikes as $k \to 1$. For smaller values of c, which we were unable to access numerically, we would expect further members of the infinite sequence of spikes to be visible in the numerical solution.

4.4. Asymptotic solution for $\phi = \tilde{\Phi}_k$ as $c \to 0$

We can provide evidence for our assertion that an infinite sequence of spikes of $O(1)$ weight emerges as $k \to 1$ when $\phi = \tilde{\Phi}_k$ by constructing the asymptotic solution as $c \to 0$. Note that in this case the TW equation (5) can be written as

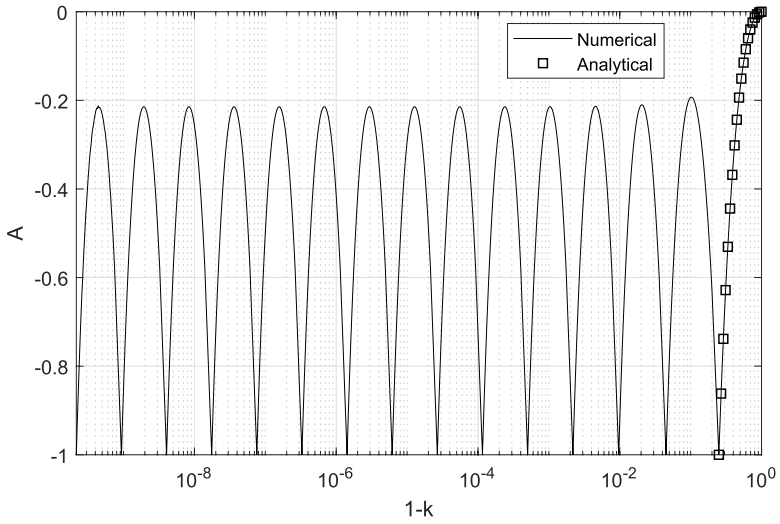

Figure 15. The function $A(k)$ plotted as a function of $1-k$. There is a sequence of points where $A+1$ is zero and a new spike is born. The squares show the analytical expression for A given by (57).

$$-cL_z = D_0c^2\left(L_{zz}+L_z^2\right)+1-(1-k)\,v_1-kv_2,$$

$$\left(1-\frac{\mathrm{d}^2}{\mathrm{d}z^2}\right)v_1=\mathrm{e}^L=U,\quad \left(1-\frac{\mathrm{d}^2}{\mathrm{d}z^2}\right)^2 v_2=\mathrm{e}^L=U. \tag{53}$$

At leading order as $c\to 0$ with $z=O(1)$ and $U,\,L=O(1)$, we find that the solution that is bounded as $z\to-\infty$ is

$$U_\infty(z;k)=1+A(k)\exp\left(\frac{z-z_M}{\sqrt{1-k}}\right). \tag{54}$$

On substituting the ansatz (52) into (3), for $z\leqslant z_M$, we obtain, at leading order as $c\to 0$, since $U>0$,

$$F(z;k)\equiv 1-\int_{-\infty}^{z_M}\left\{1+A(k)\exp\left(\frac{y-z_M}{\sqrt{1-k}}\right)\right\}\tilde{\Phi}_k(z-y)\,\mathrm{d}y$$

$$-\sum_{m=1}^{M}w_m\tilde{\Phi}_k(z-z_m)=0. \tag{55}$$

For this simple kernel, we can evaluate the integral, which gives the product of a linear factor and an exponential, and hence find two relationships between A and w_m, including

$$A\sqrt{1-k}=2-(2-k)\sum_{m=1}^{M}w_m\mathrm{e}^{z_M-z_m}, \tag{56}$$

which we will need later (see appendix for more details). For $0<k<k_1$, since $M=1$, evaluating (55) is sufficient to find the two unknowns, A and w_1, (translational invariance allows us to take $z_1\equiv 0$) as

$$w_1 = \frac{1}{\sqrt{1-k}},\ A = -\left(\frac{1}{\sqrt{1-k}} - 1\right)^2. \tag{57}$$

Since (54) shows that $U_\infty(z_M;k) = 1 + A$, we require that $A \geqslant -1$ for this single spike solution structure to be available. Using (57), this means that we need $k \leqslant \frac{3}{4}$, and hence that $k_1 = \frac{3}{4}$, consistent with the numerical solutions shown in figure 13. Note that the weight of the spike, $w_1(k)$, increases monotonically from one to two as k increases from zero to k_1. These asymptotic expressions for w_1 and A for $0 \leqslant k \leqslant k_1$ are in excellent agreement with numerical solutions of (5) (see figures 14 and 15).

For $k > k_1$ we expect multiple spikes, as given by (52), and we need to consider the asymptotic solution in the regions between the spikes, where $U \ll 1$ when $c \ll 1$. Specifically, we expect that $L = O(c^{-1})$ with $L < 0$, so that U is exponentially small in the regions between the spikes. If we define $\tilde{L} = cL$, with $\tilde{L} = O(1)$ as $c \to 0$, (note that this is a new definition, and not the notation used in section 4.1) we find that, at leading order, (5) gives

$$D_0\tilde{L}_z^2 + \tilde{L}_z + F(z;k) = 0, \tag{58}$$

with $F(z;k)$, since the ansatz (52) remains the same, given by (55), which determines $\tilde{L}_z$ in terms of F. In particular, matching to the spike regions requires $\tilde{L}_z(z_m) = 0$, and hence

$$F(z_m;k) = 0 \text{ for } m = 1, 2, \ldots, M. \tag{59}$$

It is helpful to treat these equations as a system that determines w_m for given values of z_m.

Matching also requires that $\tilde{L} = 0$ at $z = z_m$, and hence that

$$\int_{z_{m+1}}^{z_m} \tilde{L}_z \,\mathrm{d}z = 0 \text{ for } m = 1, 2, \ldots, M-1. \tag{60}$$

This can be treated as a system of equations that determines z_m for given values of w_m. For $D_0 > 0$, $\tilde{L}_z$ is related to $F(z;k)$ nonlinearly through the solution of the quadratic equation (58). However, we have found that, even for $D_0 = \frac{1}{4}$, the maximum value of D_0, which corresponds to the minimum speed TW solution, $D_0\tilde{L}_z$ is numerically very small (typically less than 0.01) in all the cases that we have studied in this paper. In other words, the solution with $D_0 = 0$ is adequate to describe, with great accuracy, the solution for $0 < D_0 \leqslant \frac{1}{4}$. As we saw in section 4.1, the term $D_0\tilde{L}_z^2$ is crucial in the region $z > 0$, ahead of the wavefront, and determines the wavespeed, but between the spikes, this diffusive term is never relevant. We therefore focus our attention on the case $D_0 = 0$, since (58) and (60) then give

$$\int_{z_{m+1}}^{z_m} F(z;k) \,\mathrm{d}z = 0 \text{ for } m = 1, 2, \ldots, M-1, \tag{61}$$

which can be evaluated analytically.

In order to determine the positions and weights of the spikes, we need to solve (56), (59) and (61). Note that (56) and (59) are linear in A and w_m, so that these variables can be eliminated. For a solution with M spikes, (61) then provides $M - 1$ nonlinear equations for the $M - 1$ distances between the spikes, Δz_m. We solve these in MATLAB using continuation in k, increasing the number of spikes in the solution by one as $A + 1$ passes through zero. Note that the linear system (59) is extremely poorly conditioned even for moderately large values of M, with the condition number of the corresponding matrix increasing exponentially with M. This is because the coefficients in (59) become very close to each other when $z_m - z_M$ is small. We were able to compute solutions with up to 18 spikes by using variable precision

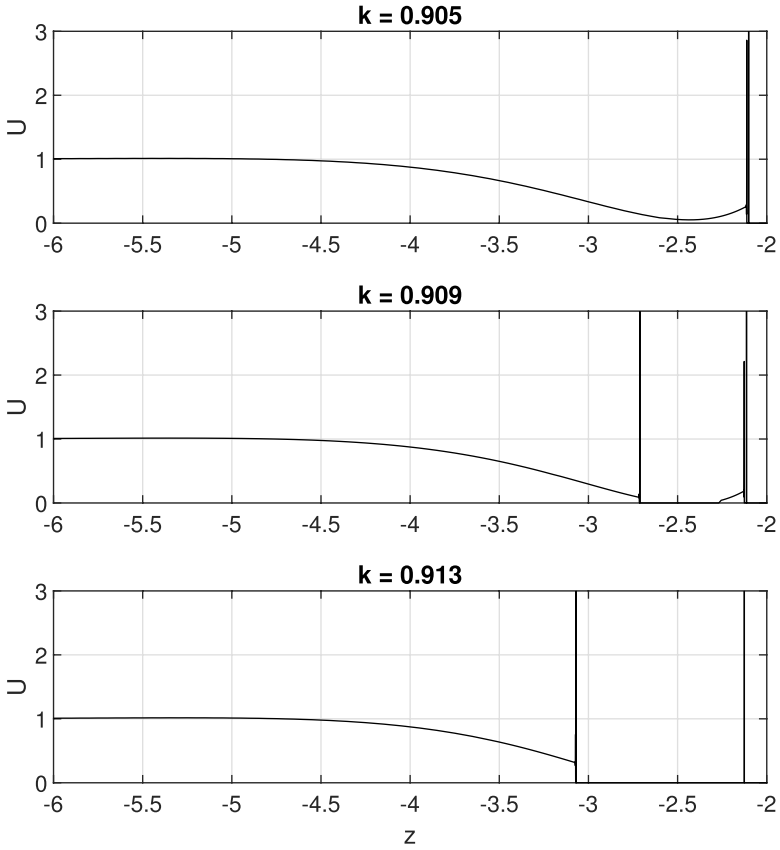

Figure 16. The TW solution for $c = 10^{-12}$ and $\phi = \bar{\Phi}_k$ for $k = 0.905$, 0.909 and 0.913.

arithmetic in MATLAB. The asymptotic solution that we calculate is shown as broken lines in figure 14. This is in excellent agreement with the numerical solution, shown as solid lines. We are able to calculate many more spikes asymptotically than we can using the full numerical solution with $c = 10^{-12}$. The function $A(k)$ is shown in figure 15, along with the analytical expression (57).

Before we move on to consider the TW solution for differentiable kernels, note that the solution for $\phi = \tilde{\Phi}_k$ described above, with a new spike being born next to the leftmost spike as k increases, and a monotonically-decreasing solution $U_\infty(z)$ behind this spike, is actually a special case. We can illustrate this by briefly considering the solution with $\phi = \bar{\Phi}_k$, given by (15). In this case, (5) can be written as the equivalent system of ordinary differential equations

$$-cL_z = D_0 c^2 \left(L_{zz} + L_z^2\right) + 1 - (1-k)\, v_1 - k v_3,$$

$$\left(1 - \frac{\mathrm{d}^2}{\mathrm{d}z^2}\right) v_1 = \mathrm{e}^L = U, \quad \left(1 - \frac{\mathrm{d}^2}{\mathrm{d}z^2}\right)^3 v_3 = \mathrm{e}^L = U. \tag{62}$$

Proceeding as we did for $\phi = \tilde{\Phi}_k$, as $c \to 0$, the leading order equation for $z < z_\infty$, where $U = U_\infty = O(1)$, is

$$(1-k)\frac{\mathrm{d}^4U_\infty}{\mathrm{d}z^4}-2(1-k)\frac{\mathrm{d}^2U_\infty}{\mathrm{d}z^2}+U_\infty=1. \tag{63}$$

In contrast to (54), the solution of (63) is not monotonic, so there is no guarantee that if it reaches zero (indicating the birth of a new spike) this will be at the position $z=z_M$ of the leftmost spike. It is possible to determine the bounded solution of (63) analytically when there is just one spike. We do not give the details here, but note that we find $k_1\approx 0.907\,94$, with the point where U_∞ reaches zero occuring away from the leftmost spike. This is consistent with the numerical solution of (5) for $c=10^{-12}$ shown in figure 16, where it is clear that U_∞ is not monotonic. Subsequent spikes are also born via this mechanism.

5. Kernels that are twice-, but not infinitely-, differentiable

We begin by discussing the governing equation in the spike regions when $\phi(x)$ is twice-, but not infinitely-, differentiable. If the first discontinuous derivative of ϕ is the pth with $p>2$ (we will discuss the case of infinitely-differentiable kernels in section 6), and if, following (40) and (41), we can write

$$\frac{\mathrm{d}^p\phi}{\mathrm{d}x^p}=-\kappa\delta(x)+\frac{\mathrm{d}^p\bar{\phi}}{\mathrm{d}x^p}, \tag{64}$$

where $\mathrm{d}^p\bar{\phi}/\mathrm{d}x^p\equiv\mathrm{d}^p\phi/\mathrm{d}x^p$ for $x\neq 0$, $\mathrm{d}^p\bar{\phi}/\mathrm{d}x^p(0)=\lim_{x\to 0^\pm}\mathrm{d}^p\phi/\mathrm{d}x^p(x)$ and

$$\kappa\equiv-2\frac{\mathrm{d}^{p-1}\phi}{\mathrm{d}x^{p-1}}(0^+), \tag{65}$$

then, after differentiating (5) p times we obtain, neglecting the diffusive terms as $c\to 0$,

$$c\frac{\mathrm{d}^{p+1}L}{\mathrm{d}z^{p+1}}+\kappa\mathrm{e}^L=\int_{-\infty}^{\infty}\frac{\mathrm{d}^p\bar{\phi}}{\mathrm{d}z^p}(z-z')\mathrm{e}^{L(z')}\mathrm{d}z'. \tag{66}$$

In the narrow spike regions, the only possible leading order balance is between the two terms on the left hand side of (66). However, for a spike with weight of $O(1)$, so that $\mathrm{e}^L=O(\mathrm{d}L/\mathrm{d}z)$, the leading order equation for $p>2$, is simply $\mathrm{d}^{p+1}L/\mathrm{d}z^{p+1}=0$, and the first p derivatives of the outer solution match across the spike region. In particular, apart from a constant correction of $O(\log c)$, the leading order solution simply reproduces the quadratic term in the inner limit of the outer expansion for $\tilde{L}\equiv cL$, and the spike is therefore Gaussian with width of $O(c^{1/2})$, weight of $O(1)$ and hence height of $O(c^{-1/2})$, all determined from matching to the outer solution, consistent with numerical solutions of the full TW problem with $c\ll 1$. The spike regions are entirely passive in terms of the asymptotic structure of the solution.

The results of section 4 suggest that when the kernel has a continuous derivative at $x=0$, an infinite number of spikes of $O(1)$ weight exist behind the wavefront, so we use an ansatz of the form

$$U(z)=U_\infty(z)H(z_\infty-z)+\sum_{m=1}^{\infty}w_m\delta(z-z_m). \tag{67}$$

We will confine our attention to the sequence of kernels $\phi=\Phi_n$, for which we can reduce the TW equation to an ordinary differential equation and $U_\infty=1$, and only consider the case of n a positive integer, even though the kernel (12) can be used in (5) for non-integer n. It would be interesting to use fractional calculus as a framework to investigate the non-integer case in detail (see (83) below), but we have not attempted this here.

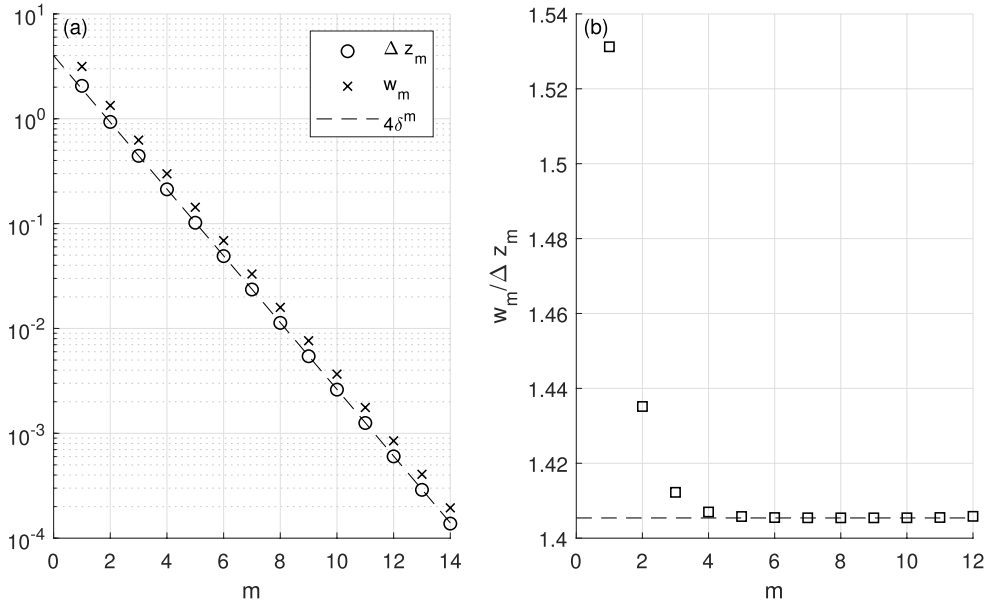

Figure 17. (a) The leading order asymptotic values of the weight, w_n, and spacing, Δz_n, of the spikes for $\phi = \tilde{\Phi}_k$ with $1 - k = 10^{-10}$. The broken line is the geometric progression $4\delta^m$, with $\delta \approx 0.4805$. This value of δ is determined analytically from the far field of the asymptotic solution (the factor of four is not). (b) The ratio of the weight, w_n, and spacing, Δz_n. The broken line is $w_\infty/\Delta z_\infty \approx 1.4054$ determined analytically from the far field of the asymptotic solution.

Guided by the analysis of the case $\phi = \tilde{\Phi}_k$ given in section 4.4, we postulate that the asymptotic solution of (5) for $c \ll 1$ when $\phi = \Phi_n$ takes the form (67) with $U_\infty = 1$ (the unique solution when $L = O(1)$ as $c \to 0$). Proceeding as before, we find that the positions and weights of the spikes are determined by the infinite system of equations

$$F(z_m) = 0 \text{ for } m = 1, 2, \ldots, \tag{68}$$

and, taking $D_0 = 0$ for the reasons discussed on page 22,

$$\int_{z_{m+1}}^{z_m} F(z)\,\mathrm{d}z = 0 \text{ for } m = 1, 2, \ldots, \tag{69}$$

where

$$F(z) \equiv 1 - \int_{-\infty}^{z_\infty} \phi(z - y)\,\mathrm{d}y - \sum_{m=1}^{\infty} w_m \phi(z - z_m). \tag{70}$$

In order to solve (68) and (69) numerically, we need to know the functional form of the far field solution, w_m and $\Delta z_m \equiv z_m - z_{m+1}$ for $m \gg 1$. We can gain some insight into this by considering the case $\phi = \Psi_2$. Note that $\Psi_2 = \tilde{\Phi}_k$ when $k = 1$.

Figure 17(a) shows w_m and Δz_m for the numerical solution of (59) and (61) when $1 - k = 10^{-10}$, which we expect to be close to the solution when $k = 1$, but with a finite number of spikes. This strongly suggests that both w_m and Δz_m decay exponentially as $m \to \infty$, and that w_m, $\Delta z_m = O(\delta^m)$ for some $0 < \delta < 1$ is an excellent approximation even

for moderate values of m. We also note from figure 17(b) that $w_m/\Delta z_m$ appears to asymptote to a constant ratio as $m \to \infty$. We can confirm this analytically for $\phi = \Psi_2 \equiv \frac{1}{4}(1+|z|)\,\mathrm{e}^{-|z|}$ and $D_0 = 0$, in which case

$$F(z) = -\tilde{L}_z = 1 - v_2, \quad \left(1 - \frac{\mathrm{d}^2}{\mathrm{d}z^2}\right)^2 v_2 = \mathrm{e}^{\tilde{L}/c}. \tag{71}$$

If we define $F_m(z)$ to be $F(z)$ for $z_{m+1} \leqslant z \leqslant z_m$, then, noting that $\mathrm{e}^{\tilde{L}/c} \ll 1$ for $\tilde{L} = O(1) < 0$, we find by solving the leading order equation $\left(1 - \frac{\mathrm{d}^2}{\mathrm{d}z^2}\right)^2 v_2 = 0$ that

$$F_m(z) = 1 + \{a_m + b_m\,(z - z_{m+1})\}\,\mathrm{e}^{z - z_{m+1}} + \{c_m + d_m\,(z - z_{m+1})\}\,\mathrm{e}^{z_{m+1} - z}. \tag{72}$$

By applying the three conditions $F_m(z_{m+1}) = F_m(z_m) = 0$ and $\int_{z_{m+1}}^{z_m} F_m(z)\mathrm{d}z = 0$, we can determine the constants a_m, b_m, c_m and d_m in terms of the as yet unknown slope $F_m'(z_{m+1})$, using computer algebra in Mathematica. Now noting that, from the definition (70), $F(z)$ is as smooth as $\phi(z - z_m)$ at $z = z_m$, we can see that F' and F'' are continuous at $z = z_m$. This leads to

$$F_{m+1}'(z_{m+1}) = F_m'(z_{m+1}), \quad F_m'(z_{m+1}) = F_m'(z_m) - f(\Delta z_m), \tag{73}$$

the first equation being simply a continuity condition and the second coming from (72) with the constants determined by computer algebra, which gives

$$f(\Delta z_m) \equiv \Delta z_m + 4\frac{\cosh \Delta z_m - 1 - \frac{1}{2}\Delta z_m^2}{\sinh \Delta z_m - \Delta z_m} \sim \frac{1}{60}\Delta z_m^3 \text{ as } \Delta z_m \to 0. \tag{74}$$

After substituting the definition of $\phi = \Psi_2$ into (70), evaluating the integral and comparing to (72) we find that

$$a_m = -\frac{1}{4}\sum_{p=1}^{m} w_p\,(1 + z_p - z_{p+1})\,\mathrm{e}^{z_{p+1} - z_p}, \; b_m = -\frac{1}{4}\sum_{p=1}^{m} w_p \mathrm{e}^{z_{p+1} - z_p},$$

$$c_m = -\frac{1}{4}\,(2 + z_{m+1} - z_\infty)\,\mathrm{e}^{z_\infty - z_{m+1}} - \frac{1}{4}\sum_{p=m+1}^{\infty} w_p\,(1 + z_{p+1} - z_p)\,\mathrm{e}^{z_p - z_{p+1}},$$

$$d_m = -\frac{1}{4}\mathrm{e}^{z_\infty - z_{m+1}} - \frac{1}{4}\sum_{p=m+1}^{\infty} w_p \mathrm{e}^{z_p - z_{p+1}}.$$

By comparing these expressions in the limit $m \to \infty$ with those that we obtained from Mathematica, we find that there are two constraints that the far field behaviour of $F_m'(z_{m+1})$ must satisfy, namely

$$F_m'(z_{m+1}) \sim \frac{1}{30}\Delta z_m^3 - \frac{1}{12}\Delta z_m^2 \sum_{p=m+1}^{\infty} (w_p - \Delta z_p)\,, \tag{75}$$

and

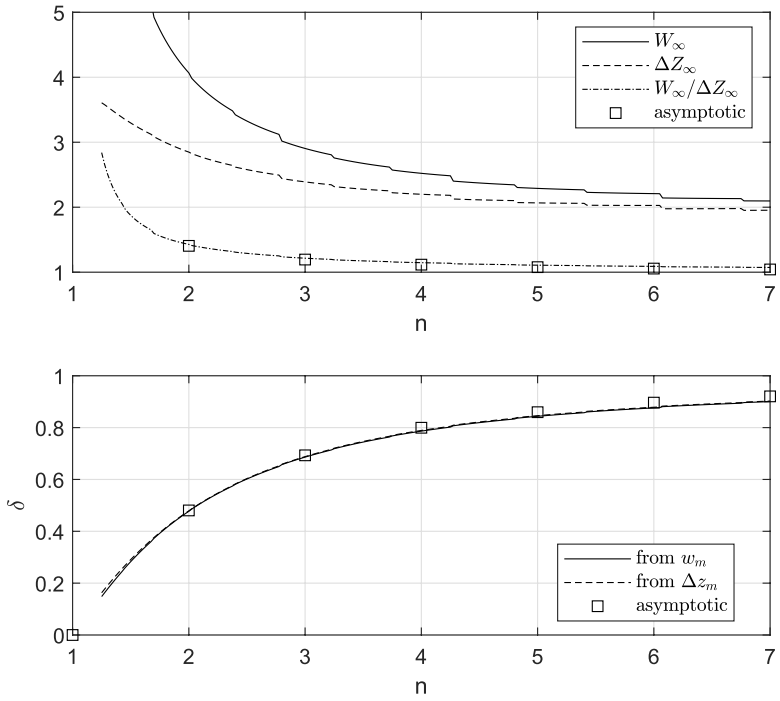

Figure 18. The upper panel shows the values of W_∞, ΔZ_∞ and their ratio as a function of n, calculated from the full numerical solution of (5) when $c = 10^{-12}$ and $\phi = \Phi_n$. The lower panel shows the value of δ calculated in the same way, either from curve fitting to w_m or Δz_m. As indicated on the figure, either method of estimating δ gives an almost identical result. In each case, the squares are the values obtained from the far field asymptotic analysis described in section 5.

$$F'_m(z_{m+1}) \sim \frac{1}{6}\left(z_{m+1} - z_\infty\right)^3 - \frac{1}{2}\sum_{p=m+1}^{\infty} w_p \left(z_p - z_{m+1}\right)^2. \tag{76}$$

Along with (73) and (74), these expressions strongly suggest that $w_m = O(\Delta z_m)$ as $m \to \infty$. If we write

$$w_m \sim W_\infty \delta^m,\ \Delta z_m \sim \Delta Z_\infty \delta^m \text{ as } m \to \infty, \tag{77}$$

and substitute into (73), (75) and (76), we find, after rearranging and summing various geometrical series, that

$$\frac{W_\infty}{\Delta Z_\infty} = 1 + \frac{2 - 3\delta^3}{5\delta\left(1 + \delta + \delta^2\right)} = \frac{(1+\delta)\left(1 + \delta + \delta^2\right)\left(-2 + \delta + 4\delta^2 + 7\delta^3\right)}{5\delta\left(-1 + \delta^2 + 7\delta^3 + 5\delta^5\right)}. \tag{78}$$

On simplifying, we find that δ is a solution of

$$\delta^4 - \delta^3 - 2\delta^2 - \delta + 1 = 0. \tag{79}$$

The only root with $0 < \delta < 1$ is

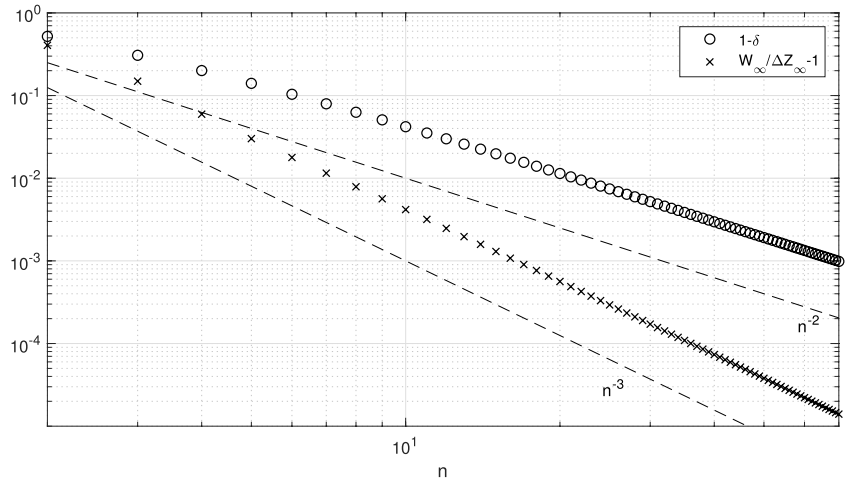

Figure 19. The behaviour of $1-\delta$ and $W_\infty/\Delta Z_\infty - 1$ as a function of n. The broken lines are $1/n^2$ and $1/n^3$.

$$\delta = \frac{1}{4}\left(1+\sqrt{17}-\sqrt{2+2\sqrt{17}}\right) \approx 0.4805, \tag{80}$$

and hence

$$\frac{W_\infty}{\Delta Z_\infty} = \frac{1}{40}\left(21+5\sqrt{17}+\sqrt{106+26\sqrt{17}}\right) \approx 1.4054. \tag{81}$$

The broken lines in figure 17 show that these constants are in excellent agreement with the numerically-calculated far field solution for $m \geqslant 5$.

This far field analysis can also be carried out for the kernels $\phi = \Psi_n$, making use of the continuity of higher derivatives of F_n. This has to be done entirely using computer algebra, and, since the polynomial that determines δ is of order greater than four for $n > 2$, no analytical expressions for the solutions are available. We find that the kernel $\phi = \Phi_n$ gives $n-1$ possible values for both δ and $W_\infty/\Delta Z_\infty$. The values corresponding to the largest value of δ in each case are plotted for $n \leqslant 7$ in figure 18. These are shown in comparison to the values obtained from the numerical solution of (5) with $c = 10^{-12}$ and $\phi = \Phi_n$ by curve fitting. These are inevitably rather crude estimates because of the limited number of spikes that emerge in each case, even for such a small value of c. However, the agreement is good, and indicates that the far field asymptotic analysis captures the behaviour of the solution. Note that figure 18 includes some results for $1 < n < 2$ that are consistent with $\delta \to 0$ and $z_\infty \to 0$ as $n \to 1$. For values of n sufficiently close to one it is difficult to resolve the tightly packed spikes that exist behind the wavefront in the full numerical solution. As $n \to \infty$, a key observation, see figure 19, is that the far field and numerical solutions strongly suggest that $\delta \to 1$ and $W_\infty/\Delta Z_\infty \to 1$, and hence that $z_\infty \to -\infty$. Recall that as $n \to \infty$, $\Phi_n(x) \to \Phi_\infty(x) \equiv \frac{1}{2\sqrt{\pi}}\mathrm{e}^{-\frac{1}{4}x^2}$. This is therefore consistent with our earlier assertion that for the Gaussian kernel, $\phi = \Phi_\infty$, the TW solution consists of an infinite sequence of spikes that fills the region $z < 0$ behind the wavefront.

Although we were able to solve (68) and (69) numerically to find w_m and Δz_m when $n = 2$, for larger values of n, the system is so ill-posed that we could not obtain a numerical solution. We were, however, able to find a numerical solution for $n = 2$, 3 and 4, but not for larger n,

by taking a different approach that does not involve w_m directly, and which also allows us to explain why the largest possible value of δ is appropriate in the far field solution. Instead of using (70) directly, we write

$$F \equiv -\tilde{L}_z = 1 - v_n, \tag{82}$$

where, for $\phi = \Phi_n$,

$$\left(1 - \frac{1}{n}\frac{\mathrm{d}^2}{\mathrm{d}z^2}\right)^n v_n = 1 + \left(1 - \frac{1}{n}\frac{\mathrm{d}^2}{\mathrm{d}z^2}\right)^n \frac{\mathrm{d}\tilde{L}}{\mathrm{d}z} = \mathrm{e}^{\tilde{L}/c}. \tag{83}$$

At leading order as $c \to 0$, in the regions, $z_{m+1} < z < z_m = z_{m+1} + \Delta z_m$ between the spikes, we therefore have

$$\tilde{L} \equiv \tilde{L}_m = A^{(m)} - (z - z_{m+1})$$

$$+ \sum_{k=1}^{n} (z - z_{m+1})^{k-1} \left(a_k^{(m)} \mathrm{e}^{n^{1/2}(z-z_{m+1})} + b_k^{(m)} \mathrm{e}^{-n^{1/2}(z-z_{m+1})}\right). \tag{84}$$

In addition, (70) shows that $\tilde{L}_z$ is as smooth as $\phi = \Phi_n$, so that

$$\frac{\mathrm{d}^p \tilde{L}_m}{\mathrm{d}z^p} = \frac{\mathrm{d}^p \tilde{L}_{m+1}}{\mathrm{d}z^p} \text{ at } z = z_m, \text{ for } p = 0, 1, \ldots 2n-1. \tag{85}$$

We must also have

$$\tilde{L}_m = \frac{\mathrm{d}\tilde{L}_m}{\mathrm{d}z} = 0 \text{ at } z = z_m, \tag{86}$$

so that the solution matches with the spike regions in the neighbourhood of $z = z_m$. This gives $2n + 2$ conditions for the $2n + 2$ unknowns, A^m, a_k^m, b_k^m and Δz_m in each region between the spikes.

For $z > z_1 = 0$, we have

$$\tilde{L}_0 = -B_1 - z + \left\{B_1 + \left(1 + n^{1/2}B_1\right) z + \sum_{k=3}^{n} B_{k-1} z^{k-1}\right\} \mathrm{e}^{-n^{1/2}z}, \tag{87}$$

which satisfies $\mathrm{e}^{\tilde{L}_0} \to 0$ as $z \to \infty$, and $\tilde{L}_0 = \mathrm{d}\tilde{L}_0/\mathrm{d}z = 0$ at $z = 0$, and involves $n - 1$ unknown constants. In order to close this system we therefore need $n - 1$ conditions as $m \to \infty$, so we must consider the far field solution.

As $m \to \infty$, $\Delta z_m \to 0$, so we rescale using

$$z = z_{m+1} + \Delta z_m \bar{z}, \ \tilde{L}_m = \Delta z_m^{2n+1} \bar{L}_m, \tag{88}$$

so that (83) with $c = 0$ becomes

$$\left(\Delta z_m^2 - \frac{1}{n}\frac{\mathrm{d}^2}{\mathrm{d}\bar{z}^2}\right)^n \frac{\mathrm{d}\bar{L}_m}{\mathrm{d}\bar{z}} = -1. \tag{89}$$

At leading order as $\Delta z_m \to 0$,

$$\left(-\frac{1}{n}\right)^n \frac{\mathrm{d}^{2n+1}\bar{L}_m}{\mathrm{d}\bar{z}^{2n+1}} = -1.$$

Since $\bar{L}_m = d\bar{L}_m/d\bar{z} = 0$ at $\bar{z} = 0$ and $\bar{z} = 1$, the solution is the polynomial

$$\bar{L}_m = \bar{z}^2 (1-\bar{z})^2 \sum_{k=1}^{2n-2} \alpha_k^{(m)} \bar{z}^{k-1}, \tag{90}$$

with

$$\alpha_{2n-2}^{(m)} = \frac{(-1)^{n+1} n^n}{(2n+1)!}. \tag{91}$$

For given values of the $2n-2$ constants Δz_m and $\alpha_k^{(m)}$, the continuity conditions (85) are

$$\Delta z_m^{2n+1-p} \frac{\mathrm{d}^p \bar{L}_m}{\mathrm{d}\bar{z}^p}\bigg|_{\bar{z}=0} = \Delta z_{m+1}^{2n+1-p} \frac{\mathrm{d}^p \bar{L}_{m+1}}{\mathrm{d}\bar{z}^p}\bigg|_{\bar{z}=1} \quad \text{for } p = 2, 3, \ldots 2n-1, \tag{92}$$

and determine Δz_{m+1} and $\alpha_k^{(m+1)}$. We can think of this as a linear recurrence relation between Δz_m and the vector

$$\boldsymbol{\alpha}_m \equiv \left(\alpha_1^{(m)}, \alpha_2^{(m)}, \ldots \alpha_{2n-2}^{(m)}\right)^{\mathrm{T}},$$

and $\boldsymbol{\alpha}_{m+1}$, with Δz_{m+1} determined nonlinearly from (91). If we define the vector of derivatives

$$\bar{\mathbf{L}}_m \equiv \left(\frac{\mathrm{d}^2 \bar{L}_m}{\mathrm{d}\bar{z}^2}, \frac{\mathrm{d}^3 \bar{L}_m}{\mathrm{d}\bar{z}^3}, \ldots \frac{\mathrm{d}^{2n-1} \bar{L}_m}{\mathrm{d}\bar{z}^{2n-1}}\right)^{\mathrm{T}}, \tag{93}$$

and a diagonal matrix Δ_m with diagonal elements

$$\left(\delta_m^{2n-1}, \delta_m^{2n-2}, \ldots \delta_m^2\right),$$

where

$$\delta_m \equiv \frac{\Delta z_{m+1}}{\Delta z_m},$$

we can write (92) as

$$\bar{\mathbf{L}}_m\big|_{\bar{z}=0} = \Delta_m \, \bar{\mathbf{L}}_{m+1}\big|_{\bar{z}=1}. \tag{94}$$

Since (90) is linear in $\alpha_k^{(m)}$, we can also write

$$\bar{\mathbf{L}}_m\big|_{\bar{z}=0,1} = M_{0,1} \boldsymbol{\alpha}_m, \tag{95}$$

where $M_{0,1}$ are two $(2n-2) \times (2n-2)$, constant, square matrices that can be calculated from (90) (using computer algebra for large n). For example, when $n = 2$,

$$M_0 = \begin{pmatrix} 2 & 0 \\ -12 & 6 \end{pmatrix}, \quad M_1 = \begin{pmatrix} 2 & 2 \\ 12 & 18 \end{pmatrix}.$$

We can now write

$$M_0 \boldsymbol{\alpha}_m = \Delta_m M_1 \boldsymbol{\alpha}_{m+1}. \tag{96}$$

For given $\boldsymbol{\alpha}_m$ we can solve (96) to find $\boldsymbol{\alpha}_{m+1}$, and then (91) fixes δ_m. Equilibrium solutions have $\boldsymbol{\alpha}_{m+1} = \boldsymbol{\alpha}_m$, and $\delta_m = \delta$, which can be found from $\det(M_0 - \Delta M_1) = 0$. This leads to the same $n-1$ values of δ that we found in section 5. We also note that

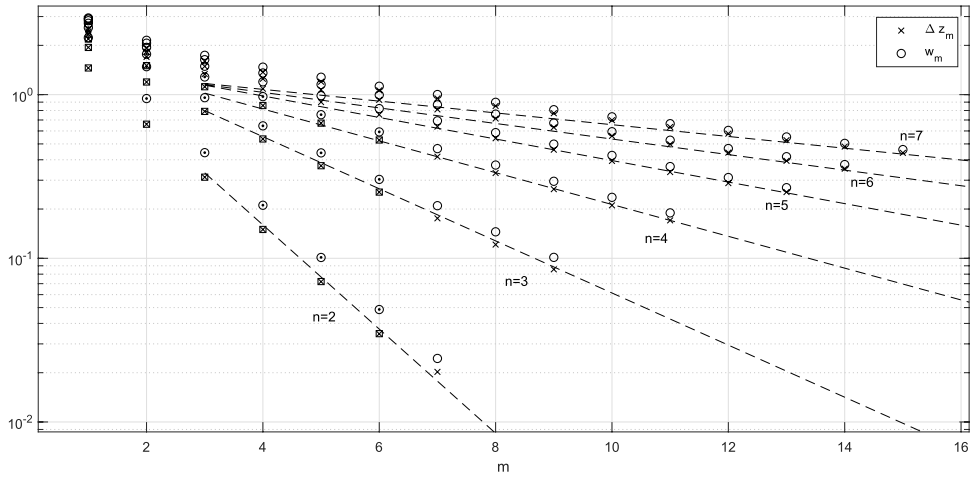

Figure 20. The spacing, Δz_m, and weight, w_m of the spikes for $n \leqslant 7$, determined from the numerical solution (crosses and circles) and the asymptotic solution (dots and squares). The broken lines have slope given by δ, calculated from the far field asymptotic solution.

$$\frac{W_\infty}{\Delta Z_\infty} = (-n)^{-n}\left(\frac{1}{\delta}\frac{\mathrm{d}^{2n}\bar{L}}{\mathrm{d}\bar{z}^{2n}}\bigg|_{\bar{z}=0} - \frac{\mathrm{d}^{2n}\bar{L}}{\mathrm{d}\bar{z}^{2n}}\bigg|_{\bar{z}=1}\right)$$

$$= 1 + \frac{1-\delta}{\delta}\left(\frac{(2n)!}{(-n)^n}\alpha_{2n-3} + \frac{2}{2n+1}\right).$$

It is also straightforward, using computer algebra, to linearise (91) and (96) about the equilibrium solution and find that each of the $n-1$ equilibrium solutions has a stable manifold of a different dimension. In order to solve numerically, we truncate at large, finite m and need $n-1$ boundary conditions, one of which is to specify Δz_m, so we need the solution with an $(n-2)$-dimensional stable manifold. This, consistent with numerical solutions of the TW equation, is the solution with the largest value of δ. This gives us enough information to be able to solve the nonlinear system of equations given by (84) to (87) using *fsolve* in MATLAB. We used the Advanpix multiprecision computing toolbox, [13], to increase the precision of the computation, up to 66 digits of accuracy for $n = 4$. For $n > 4$ the system was too stiff for convergence to be achieved. The results, which are in excellent agreement with full numerical solutions of (5), are shown in figure 20, along with the far field behaviour indicated by Δz_m, $w_m = O(\delta^m)$.

We note that neither of the two numerical approaches described above is entirely satisfactory, and further work is required to devise a method better suited to this challenging system of equations. We have included these brief details of both methods here, since the former is more intuitive and leads naturally to the analytical results noted above, whilst the latter is more numerically stable.

Finally, we note that the case $\phi = \Phi_n$ is unusual since it has $U_\infty = 1$. A more typical solution, with a kernel that is a linear combination of the Gaussian, Φ_∞, and Ψ_2, is shown in figure 21. For $z < z_\infty \approx 17$, U is oscillatory. This solution would be very hard to understand without the context provided by the preceding analysis.

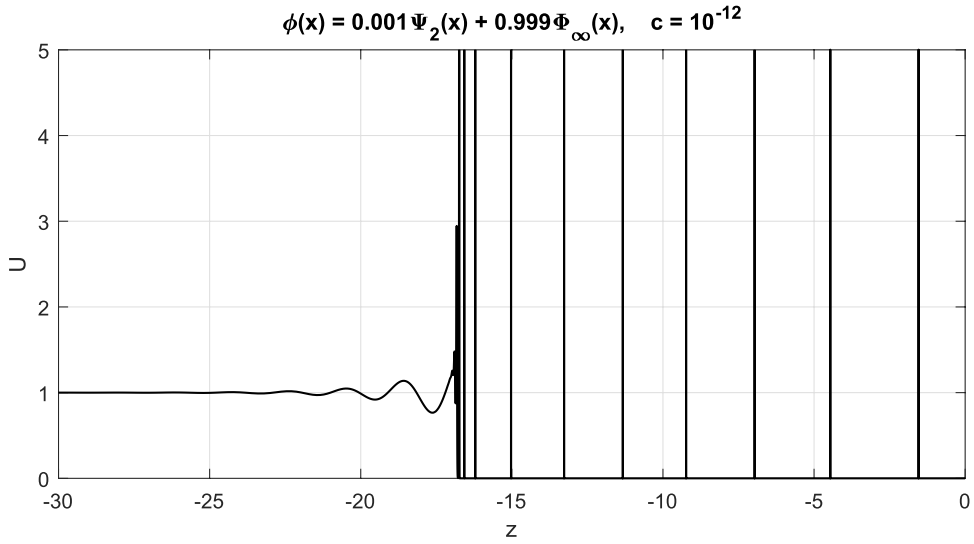

Figure 21. The TW solution of (5) when $c = 10^{-12}$ and $\phi = 0.999\Psi_2(x) + 0.001\Phi_\infty(x)$.

6. Infinitely-differentiable kernels

When the kernel, ϕ, is infinitely-differentiable, the results of section 5, specifically that $\delta \to 1$ as $n \to \infty$, indicate that $z_\infty \to -\infty$ as $n \to \infty$, and that for $\phi = \Phi_\infty$ and other infinitely-differentiable kernels, the whole of the region behind the wavefront is filled with spikes in the limit $c \to 0$. There is no obvious way to determine the large n asymptotic limit of the TW solution when $\phi = \Phi_n$, specifically the solution of (89) when $n^{-1} \ll \Delta z_m \ll 1$, and the limit $n \to \infty$ for (83) may not be well-defined, as discussed in [14].

Taking all of this into account, an appropriate ansatz for infinitely-differentiable kernels is

$$U(z) = \sum_{m=1}^{\infty} w_m \delta(z - z_m), \tag{97}$$

and hence

$$-\tilde{L}_z = 1 - \sum_{m=1}^{\infty} w_m \phi(z - z_m). \tag{98}$$

After integrating (98), it is convenient to write the solution as

$$\tilde{L} = A - z + \sum_{m=1}^{\infty} w_m \left\{ I(z - z_m) - 1 \right\}, \tag{99}$$

with A a constant and

$$I(z) \equiv \int_{-\infty}^{z} \phi(z')\mathrm{d}z'.$$

Since $I(z - z_m) \to 0$ as $z \to -\infty$, this means that $w_m \sim \Delta z_m$ as $m \to \infty$ and $A = \sum_{m=1}^{\infty} (w_m - \Delta z_m)$, so that

$$\tilde{L} = -z + \sum_{m=1}^{\infty} \{w_m I(z - z_m) - \Delta z_m\}. \tag{100}$$

Note that this is consistent with the result $W_\infty \sim \Delta Z_\infty$ as $n \to \infty$ (see figure 19). The conditions $\tilde{L} = \tilde{L}_z = 0$ at each spike then lead to the infinite system of nonlinear equations

$$\sum_{m=1}^{\infty} w_m \phi(z_p - z_m) = 1, \tag{101}$$

$$\sum_{m=1}^{\infty} \{w_m I(z_p - z_m) - \Delta z_m\} = z_p, \quad \text{at } z = z_p \text{ for } p = 1, 2, \ldots, \tag{102}$$

for Δz_m and w_m. Since there is no ordinary differential equation that determines $\tilde{L}$, solving (101) and (102) is the only way to investigate the behaviour of the spikes for infinitely-differentiable kernels. In order to do this numerically, we need to quantify the behaviour of the far field solution. Although we have seen that $\Delta z_m \sim w_m$ as $m \to \infty$, it is not clear how to determine the individual behaviour of Δz_m and w_m. We can, however, show that Δz_m cannot asymptote to a constant as $m \to \infty$.

For $p \gg 1$, (101) becomes at leading order

$$G \equiv \sum_{m=1}^{\infty} \Delta z_m \phi(z_p - z_m) - 1 = 0. \tag{103}$$

However, $\int_{-\infty}^{\infty} \phi(z)\mathrm{d}z = 1$, so, for $p \gg 1$, (103) is equivalent to a simple discretization of this integral, and if $\Delta z_m \to \Delta z_\infty$, a constant, as $m \to \infty$, this is the trapezium rule, which is spectrally-accurate for integrals of analytic functions along the real axis, [15]. For example, when $\phi = \Phi_\infty$, $G \sim 2\mathrm{e}^{-4\pi^2/\Delta z_\infty^2}$ as $\Delta z_\infty \to 0$. A similar result holds for the smooth exponentially- and algebraically-decaying kernels

$$\Phi_{\mathrm{exp}} \equiv \frac{1}{4}\mathrm{sech}^2\left(\frac{1}{2}x\right), \ \Phi_{\mathrm{alg}} \equiv \frac{2}{\pi(1+x^2)^2}, \tag{104}$$

that we study below, with the exponential rate at which G tends to zero controlled by the distance of the poles of ϕ from the real axis, [15]. Numerical calculation for these three kernels shows that in each case G is strictly positive, so that a far field solution of (101) cannot have a constant spacing of the spikes. We will see below that there is strong numerical evidence that Δz_m decays algebraically fast as $m \to \infty$, but we cannot prove this.

Fortunately, $\Delta z_m \sim w_m$ as $m \to \infty$ is enough information about the far field to allow us to truncate the infinite set of equations (101) and (102) and solve them numerically, although we will see that the crude approximation to the far field that we use introduces a significant error into the solution. We first reinstate the constant A defined in (99) and write (102) as

$$\sum_{m=1}^{\infty} w_m \bar{I}(z_p - z_m) = A - z_p, \quad \text{at } z = z_p \text{ for } p = 1, 2, \ldots, \tag{105}$$

where

$$\bar{I}(z) \equiv \int_z^{\infty} \phi(z')\mathrm{d}z'.$$

We now note that

$$\sum_{m=M+1}^{\infty} w_m\phi(z_p - z_m) \sim \sum_{m=M+1}^{\infty} \Delta z_m\phi(z_p - z_m) \sim \int_{z_p - z_{M+1}}^{\infty} \phi(y)\mathrm{d}y, \text{ as } m \to \infty.$$

Using a similar approach for (105), we truncate the infinite set of equations as

$$\sum_{m=1}^{M} w_m\phi(z_p - z_m) \approx 1 - \int_{z_p - z_{M+1}}^{\infty} \phi(y)\mathrm{d}y, \tag{106}$$

$$\sum_{m=1}^{M} w_m\bar{I}(z_p - z_m) \approx A - z_p - \int_{z_p - z_{M+1}}^{\infty} \bar{I}(y)\mathrm{d}y, \text{ at } z = z_p \text{ for } p = 1, 2, \ldots, M. \tag{107}$$

This is a set of $2M$ equations in the $2M$ unknowns A, w_m for $m = 1, 2, \ldots, M$ and Δz_m for $m = 1, 2, \ldots, M-1$. We solve the nonlinear system for A and Δz_m numerically in MATLAB using *fsolve*, solving the linear system for A and w_m using *linsolve*. We begin with $M = 2$, for which a crude inital guess converges rapidly to a solution, and then successively increase M by one, with an initial guess of the solution formed by extending the vector Δz_m obtained for the previous value of M.

Figure 22 shows the spacing and weight of the spikes for the smooth kernels Φ_∞, Φ_{sech} and Φ_{alg}, calculated both from the full numerical solution of (5) and from the asymptotic solution, calculated numerically from (106) and (107). We find that the asymptotic solution reproduces the numerical solution, but that the inaccurate far field approximation discussed above leads to large errors for $m > \frac{1}{2}M$. In each case, the spacings that we are able to compute are not inconsistent with the region behind the wavefront being completely filled with spikes as $c \to 0$, since it appears that $1 \gg \Delta z_m \gg m^{-1}$ as $m \to \infty$. In addition, there is numerical evidence that for the Gaussian kernel, $\phi = \Phi_\infty$, an entire function, $\Delta z_m = O(m^{-1/4})$ as $m \to \infty$, whilst for the other two kernels, which have poles, at $x = \pm i\pi$ for Φ_{exp} and at $x = \pm i$ for Φ_{alg}, $\Delta z_m = O(m^{-1/2})$ as $m \to \infty$. Moreover, we speculate that it is the position of the poles nearest to the real axis that controls this rate of decay, drawing on the results of [15], and as suggested by figure 22.

7. Conclusion

In this paper we have studied the structure of slow travelling wave solutions of the nonlocal Fisher equation, (1), when the diffusivity, D, and hence minimum wavespeed, $c = c_{\text{min}} \equiv 2\sqrt{D}$, is small. For all the kernels that we used, the obvious common feature is the existence of one or more large, narrow spikes, with height of $O(c^{-1/2})$ and width of $O(c^{1/2})$. The number and spacing of these spikes depend crucially on the behaviour of the kernel, $\phi(x)$, in the neighbourhood of $x = 0$. Kernels with a discontinuous derivative at $x = 0$ lead to travelling wave solutions with a finite number of spikes. Kernels that are differentiable, but not infinitely-differentiable, lead to an infinite number of spikes that fill a finite region behind the wavefront. Infinitely-differentiable kernels lead to infinitely-many spikes that extend to infinity behind the wavefront. Although we were able to obtain detailed information about the solution for kernels that are not too smooth, the leading order problem for $c \ll 1$ when the order of the discontinuous derivative of the kernel is greater than around eight is too poorly conditioned for the numerical methods that we developed to converge to a solution. For infinitely-differentiable kernels, we have been unable to determine analytically from the leading order equations any information about the far field behaviour of the spikes beyond $w_m \sim \Delta z_m$ as $m \to \infty$ (the weight

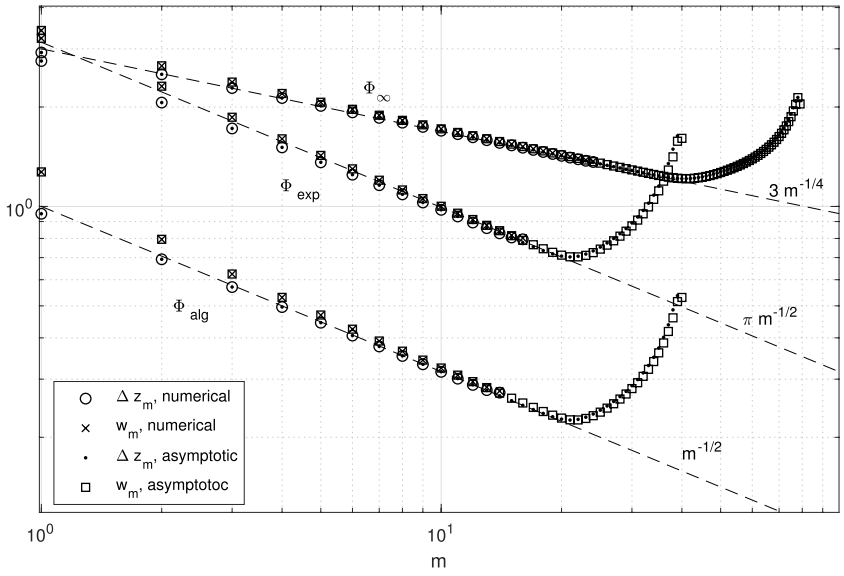

Figure 22. The weight and spacing of the spikes determined numerically from (5) when $c = 10^{-10}$ and asymptotically from (106) and (107) for the smooth kernels $\phi = \frac{1}{\pi(1+x^2)}$, $\frac{1}{4}\mathrm{sech}^2\left(\frac{1}{2}x\right)$, $\frac{1}{2\sqrt{\pi}}\mathrm{e}^{-\frac{1}{4}x^2}$. The approximate algebraic rate of decay of $\Delta z_m \sim w_m$ as $m \to \infty$ suggested by these results in each case is shown by broken lines.

and spacing of the spikes become identical in the far field), although numerical solutions of both the full travelling wave equation and the asymptotic solution for $c \ll 1$ suggest that the weight and spacings of the spikes decay algebraically-fast as $z \to -\infty$, and we speculate that the position of the poles of the kernel in the complex plane may be the controlling factor. The results that we have obtained in this paper are summarized in table 1.

One interpretation of the solutions that we have studied here when $c \ll 1$, using both numerical and asymptotic methods, is as nontrivial, steady state solutions of the nonlocal Fisher-KPP equation, (1), for $D = 0$, since they satisfy $u(x)\left(1 - \int_{-\infty}^{\infty}\phi(x-y)\,u(y)\,\mathrm{d}y\right) = 0$. The limit $D \to 0$ is, as we have demonstrated, singular, but it is worth considering whether such steady state solutions could be relevant in physical situations for which the nonlocal Fisher-KPP is appropriate.

We now consider possible futher work related to the nonlocal Fisher-KPP equation that is suggested by the results presented in this paper. The use of fractional calculus to study travelling wave solutions when $\phi = \Phi_n$ for non-integer n, for example in (83), would be interesting, and could shed some light on the issue of convergence to a Gaussian kernel as $n \to \infty$. Other extensions of this analysis could include kernels $\phi(x)$ that are non-monotonic, non-positive and/or discontinuous in $x > 0$; such kernels are used extensively in theoretical neuroscience, [16]. The extension of our analysis to two spatial dimensions is challenging, but would also be of interest.

Throughout the paper we have used asymptotic and numerical methods to gain insight into the travelling wave solutions. Our analysis lacks rigour, not only because of a lack of expertise, but also because the limit $D \to 0$ is far from that where rigorous results are currently available, namely $D \to \infty$, where the nonlocal Fisher-KPP equation asymptotes to the

standard, local Fisher-KPP equation, [9]. It seems clear that subtle features of the kernel control the gross features of the solution when $D \ll 1$, and that the methods of modern nonlinear functional analysis could provide a route to a deeper understanding of this relationship.

Acknowledgments

I would like to thanks my colleagues Daniele Avitabile and Stephen Coombes, and David Needham and John Meyer from the University of Birmingham for helpful comments and discussions.

Appendix. Asymptotic solution for $\phi = \tilde{\Phi}_k$ as $c \to 0$—detailed calculations

If we substitute the definition of $\tilde{\Phi}_k(x) \equiv \left\{\frac{1}{2}(1-k) + \frac{1}{4}k(1+|x|)\right\} \mathrm{e}^{-|x|}$ into (55) and evaluate the integral analytically for $z < z_M$, we obtain

$$\frac{1}{4}\mathrm{e}^{-z_M}\left[-2 + A\sqrt{1-k} + \left\{k + A\left(k - 1 - \sqrt{1-k}\right)\right\}(z - z_M)\right] + \ldots$$

$$\sum_{m=1}^{M} w_m \mathrm{e}^{-z_m}\left\{\frac{1}{2} - \frac{1}{4}k - \frac{1}{4}k(z - z_m)\right\} = 0. \tag{A.1}$$

Since this must hold for all $z < z_M$, we have

$$\frac{1}{4}\mathrm{e}^{-z_M}\left\{k + A\left(k - 1 - \sqrt{1-k}\right)\right\} - \frac{1}{4}k\sum_{m=1}^{M} w_m \mathrm{e}^{-z_m} = 0, \tag{A.2}$$

and

$$\frac{1}{4}\mathrm{e}^{-z_M}\left(-2 + A\sqrt{1-k}\right) + \left(\frac{1}{2} - \frac{1}{4}k\right)\sum_{m=1}^{M} w_m \mathrm{e}^{-z_m} = 0. \tag{A.3}$$

Note that (A.3) can be rearranged to give (56).

When $0 < k < k_1$, $M = 1$ and translational invariance allows us to take $z_1 = 0$, so that (A.2) and (A.3) become

$$\frac{1}{4}\left\{k + A\left(k - 1 - \sqrt{1-k}\right)\right\} - \frac{1}{4}kw_1 = 0, \tag{A.4}$$

and

$$\frac{1}{4}\left(-2 + A\sqrt{1-k}\right) + \left(\frac{1}{2} - \frac{1}{4}k\right)w_1 = 0. \tag{A.5}$$

Solving (A.4) and (A.5) for w_1 and A gives (57).

ORCID iDs

John Billingham https://orcid.org/0000-0002-4392-5770

References

[1] Nadin G, Perthame B and Tang M 2011 *C. R. Math.* **349** 553–7
[2] Faye G and Holzer M 2015 *J. Differ. Equ.* **258** 2257–89
[3] Britton N 1990 *SIAM J. Appl. Math.* **50** 1663–88
[4] Furter J and Grinfeld M 1989 *J. Math. Biol.* **27** 65–80
[5] Volpert V 2014 *Elliptic Partial Differential Equations: Volume 2: Reaction–Diffusion Equations* (Basel: Springer) pp 521–626
[6] Berestycki H, Nadin G, Perthame B and Ryzhik L 2009 *Nonlinearity* **22** 2813
[7] Coville J and Dupaigne L 2007 *Proc. R. Soc. Edinburgh* A **137** 727–55
[8] Alfaro M and Coville J 2012 *Appl. Math. Lett.* **25** 2095–9
[9] Gourley S 2000 *J. Math. Biol.* **41** 272–84
[10] Gierer A and Meinhardt H 1972 *Kybernetik* **12** 30–9
[11] Perthame B and Génieys S 2007 *Math. Model. Nat. Phenom.* **2** 135–51
[12] Billingham J 2007 *IMA J. Appl. Math.* **73** 4–36
[13] Advanpix LLC *Multiprecision computing toolbox for MATLAB* (Yokohama, Japan, 2008–2020) (www.advanpix.com)
[14] Carlsson M, Prado H and Reyes E G 2016 *Ann. Henri Poincaré* **17** 2049–74
[15] Trefethen L and Weideman J 2014 *SIAM Rev.* **56** 385–458
[16] Coombes S, Graben P, Potthast R and Wright J 2014 *Neural Fields: Theory and Applications* (New York: Springer)